J. Appl. Comput. Mech., 11(2) (2025) 327-343
DOI: 10.22055/jacm.2024.47226.4679

ISSN: 2383-4536
jacm.scu.ac.ir

Shahid Chamran
University of Ahvaz

Journal of
Applied and Computational Mechanics

Research Paper

Static Bending Analysis of Nanobeam-Substrate Medium Systems Incorporating Mixture Stress-Driven Nonlocality, Surface Energy, and Substrate-Structure Interactions

Suchart Limkatanyu[1], Worathep Sae-Long[2], Jaroon Rungamornrat[3], Nattapong Damrongwiriyanupap[2], Suraparb Keawsawasvong[4], Piti Sukontasukkul[5], Chayanon Hansapinyo[6]

[1] Department of Civil and Environmental Engineering, Faculty of Engineering, Prince of Songkla University, Songkhla, 90110, Thailand, Email: suchart.l@psu.ac.th

[2] Civil Engineering Program, School of Engineering, University of Phayao, Phayao, 56000, Thailand, Email: worathep.sa@up.ac.th (W.S.L.); nattapong.da@up.ac.th (N.D.)

[3] Applied Mechanics and Structures Research Unit, Department of Civil Engineering, Faculty of Engineering, Chulalongkorn University, Bangkok 10330, Thailand, Email: jaroon.r@chula.ac.th

[4] Research Unit in Sciences and Innovative Technologies for Civil Engineering Infrastructures, Department of Civil Engineering, Faculty of Engineering, Thammasat School of Engineering, Thammasat University, Pathumthani, 12120, Thailand, Email: ksurapar@engr.tu.ac.th

[5] Construction and Building Materials Research Center, Department of Civil Engineering, King Mongkut's University of Technology North Bangkok, Bangkok, 10800, Thailand, Email: piti.s@eng.kmutnb.ac.th

[6] Center of Excellence in Natural Disaster Management, Department of Civil Engineering, Chiang Mai University, Chiang Mai, 50200, Thailand, Email: chayanon@eng.cmu.ac.th

Received June 21 2024; Revised July 22 2024; Accepted for publication July 24 2024.
Corresponding author: W. Sae-Long (worathep.sa@up.ac.th)

Abstract. This paper proposes a novel nonlocal beam-substrate model for the static bending analysis of a nanobeam system on a substrate medium. The proposed model incorporates the coupling interaction among nonlocality, surface energy, and substrate-structure interaction. The mixture stress-driven nonlocal model is used to capture the material's small-scale effects inherent in micro- and nanoscale systems, resulting in well-posed micro- and nanostructure responses. The Gurtin-Murdoch continuum surface-energy model and the Winkler foundation model, which respectively represent size-dependent and substrate-structure interaction effects, are considered. The governing differential equation (GDE) and its relevant boundary conditions are derived based on the displacement-based principle. The analytical solutions are directly obtained from the GDE and employed to assess the bending responses. To demonstrate the impact of the mixture parameter, surface energy, and substrate-structure interaction on the static bending analysis of nanobeam systems, four numerical simulations are conducted. The first simulation validates the proposed nanobeam system by comparing it to experimental results, while the second simulation demonstrates the impact of surface energy and substrate-structure interaction on beam deflection. The third and fourth simulations analyze the impact of different system variables on the normalized transverse displacement and effective bulk Young's modulus (EBYM), respectively. The analysis results demonstrate that material nonlocality caused by the mixture parameter and length-scale parameter, as well as surface energy and substrate-structure interaction effects, impact the bending behaviors of the nanobeam systems.

Keywords: Mixture parameter, Eringen's integral elasticity, Small-scale effect, Bending analysis, Surface-energy effect.

1. Introduction

In the present day, a wide range of advanced materials and tiny-scale structures have attracted interest and have been applied in engineering, resulting in the revolution of several novel applications, such as carbon nanotubes [1], biosensors [2], nanogenerators [3], energy harvesters [4], and DNA-based sensors [5]. To support these developments, deep knowledge of the characteristics and behaviors of these applications is required, which will be a challenging task for the researchers. However, as reported in several publications [6-12], the classical elasticity theory is incapable of representing the size-scale effects inherent in micro- and nano-sized structures. Furthermore, experiments at small scales, particularly those at the micro- and nanoscale dimensions, are extremely difficult to carry out [13-15]. As a result, developing rational structural models to predict complex micro- and nanostructural properties is a consistent option, and this work is motivated by this.

Published online: July 29 2024

Generally, there are three alternative modeling approaches for micro- and nanostructures, namely the atomistic models [16-17], the continuum models [18-20], and the mixture of atomistic and continuum mechanics [21-22]. Based on their time consumption, atomistic-based approaches and mixtures of atomistic and continuum mechanics are less popular than continuum models due to their complexity and the discrete nature of matter. As a result, this leads to a high computational effort [23-26]. Thus, the continuum modeling approach is an excellent choice because it is highly accurate but also simple. Until date, the non-classical continuum models have been enhanced and utilized, together with higher-order elasticity theories, to investigate the static and dynamic mechanical characteristics of micro- and nanostructures [27-35].

In these higher-order elasticity theories, Eringen [36-37] developed the nonlocal elasticity theory as a higher-order elasticity theory. This theory is commonly employed to explain the small-scale effect caused by the discrete nature of matter within micro- and nano-sized structures [18, 38-42]. The principle and first idea of the nonlocal elasticity theory is known as "*strain-driven nonlocal elasticity*," as probably proposed by Kröner [43], Krumhansl [44], and Kunin [45]. However, this theory is complicated and has a high computational cost to apply due to the existing stress-strain relation in terms of the integral form. To overcome these limitations, Eringen [37] provided the equivalent differential form of this theory for one-dimensional homogeneous and isotropic elastic materials. Based on its simplicity, differential nonlocal elasticity has been employed to study both the static and dynamic mechanical behaviors of micro- and nanostructures over the last two decades [18, 38-42]. However, there are some analytical cases with the vanishing of the small-scale effect obtained from the equivalent differential form of this theory [37], such as a cantilever beam system subjected to a free-end point load [46-48] and subjected to a purely coupled load at a free-end boundary [11, 49], as reported in the literature [11, 46-49]. This inconsistency is later defined as a "*paradox*," and it leads to irrational responses within micro- and nanostructures [50-51]. Romano et al. [50] and Fernández-Sáez et al. [51] revealed the paradoxical results inherent in the differential nonlocal elasticity caused by the incompatibility boundary conditions. To avoid this mathematical problem, the Eringen nonlocal integral theory with accounting for a two-phase mixture defined by a combination of local and nonlocal states is an alternative way leading to the well-posed structural-mechanics problems, as shown in the literature [52-56]. There are two general approaches for the two-phase mixture nonlocal model, namely the strain-driven two-phase integral models [56-57] and the stress-driven two-phase integral models [53-55]. The first one assumes the nonlocal stress is a function of the convolution integral between elastic strain and the averaging kernel function, while the second one assumes the strain depends on the convolution integral between stress and the averaging kernel. As reported by Romano et al. [58], Eringen's strain-driven mixture for bounded structures is just a partial constitutive solution for the ill-posedness of Eringen's strain-driven purely nonlocal model. Indeed, a singular behavior in the case of the vanishing local phase still appears, and the structural ill-posedness of Eringen's entirely nonlocal theory is not totally resolved. On the other hand, the stress-driven two-phase integral model does not suffer from these limitations and leads to the well-posed nonlocal models, as presented in the literature [53-56, 59, 60]. Therefore, based on the excellent merit of this approach, this work employs the stress-driven two-phase integral model to account for the small-scale effect inherent in micro- and nano-sized structures.

The size-dependent effect refers to the influence of surface stress and elasticity on the mechanical properties of micro- and nano-sized structures. This effect is induced by the free energy of the surface around the structure. Simulations and tests have reported this phenomenon [61-68]. When the scale's dimension approaches the micro- or nano-size, the different energies at the bulk and at the free surface are comparable and cannot be ignored due to the raised surface-to-volume ratio. This phenomenon is defined as the "*surface-energy effect*" and represents a size-dependent effect inherent to micro- and nanostructures. In order to account for this effect within the structural continuum models, Gurtin and Murdoch [61-62] introduced the surface continuum theory, which was enhanced from the surface theory of Cammarata [63]. In this surface continuum model, the surface layer is assumed to wrap the bulk-solid core with a zero-thickness and perfect bond. As a result of these simple hypotheses, this model was extensively used to represent the size-dependent effect within the continuum structural models [9, 11, 18, 19, 28, 32, 48, 64-68].

Over the last few decades, one of the engineering applications that has been of interest to the research community is micro- and nanostructures resting on an elastic foundation [9, 11, 18, 19, 28, 32, 34, 40, 48, 69-73]. For the basic concept employed to simulate the elastic foundation, the Winkler foundation model [74] is one of the simplest and most extensively used models to address the underlying substrate-structure interaction with the discrete spring series. Based on its simple assumptions, there are several works that employ the Winkler model to study the behavior and characteristics of micro- and nanobeam systems resting on the elastic substrate medium [9, 11, 18, 19, 28, 32, 34, 40, 48, 69-74]. For example, Limkatanyu and co-workers [9, 11, 18, 19, 32, 48, 57] employed the Winkler foundation to develop and simulate the interaction between substrate-nanobar interaction [9, 18, 19, 32] and substrate-nanobeam interaction [11, 48, 57]. Lignola et al. [40] developed and proposed a closed-form solution for the bending of the Eringen nonlocal Timoshenko beam system on an elastic medium due to the shear deformation for static bending analysis. Demir et al. [69] used Eringen's nonlocal elasticity theory and the Winkler foundation model to develop a beam-substrate model for the static analysis of nanobeam systems resting on foundations using the finite element method. Togun and Bagdatli [70] proposed the modified couple-stress beam model on the Winkler foundation to investigate the scale effect on the free vibration of nanobeams on the foundation, while Luo et al. [71] employed that using the nonlocal strain gradient theory to study the free vibration of piezoelectric sandwich nanobeams on the foundation. Karmakar and Chakraverty [72] enhanced the beam model on the substrate medium with the nonlocal strain gradient theory by using the Adomian decomposition method (ADM) and homotopy perturbation method (HPM) to find solutions for the thermal vibration analysis of a nonhomogeneous nanobeam on foundation. Zheng et al. [73] improved the beam on the Winkler model by incorporating Reddy's third-order shear deformation theory (RTSDT) and nonlocal elasticity theory. This was done to analyze the bending behavior of a three-layer magneto-electro-elastic (MEE) laminated nanobeam that is supported by an elastic foundation. The study also took into account the nonlinear geometric effect. Furthermore, nonlocal beam models on two-parameter foundations have been developed and proposed [75-76]. For example, Ghazwani et al. [75] analyzed high-frequency functionally graded sandwich nanobeams on elastic foundations, considering both hard-core and soft-core structures. Subsequently, they extended their work to examine the frequency behaviors of nanobeams with exponential grading supported by Winkler-Pasternak foundations [76]. All of those works mentioned above confirmed and demonstrated the importance and impact of the interaction between structure and foundation for both static and dynamic analysis of the nanobeam systems resting on an elastic substrate medium. However, the stress-driven two-phase integral model, to the best of the authors' knowledge, has not yet been integrated into the beam-substrate medium model. As a result, there is still opportunity for the rational beam-substrate medium model to be developed within the research community.

The rest of this work is structured as follows: The "*Methods*" section demonstrates the fundamental concept of the model formulation for the nanobeam model on substrate medium. Next, the "*Results and Discussion*" section is employed to study and show the effect of the mixing parameter and system parameters on the behaviors of the nanobeam systems on the substrate medium. Finally, all observations are summarized in the "*Conclusion*" section.

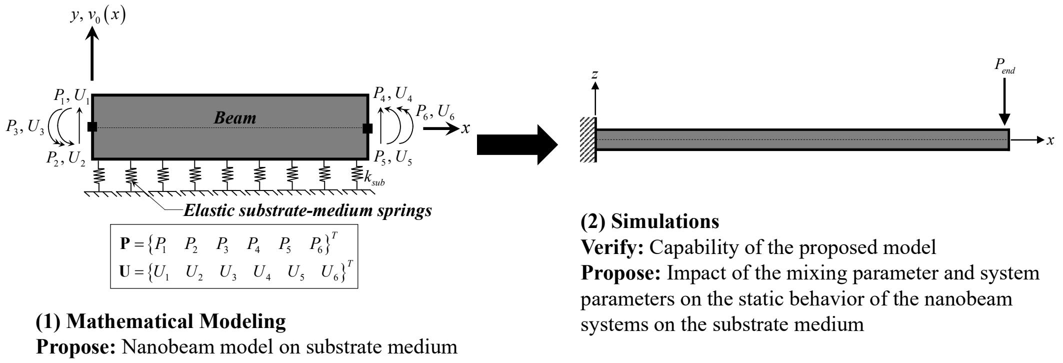

Fig. 1. Research methodology.

2. Methods

Out of all the previously mentioned research directions, the main objective of this paper is to develop and propose a novel beam-substrate medium model based on the stress-driven two-phase integral model together with the Gurtin-Murdoch surface elasticity theory [61-62] for the static bending analysis of the nanobeam systems resting on the elastic substrate medium. The beam kinematic hypothesis relies on the principles of the Euler-Bernoulli beam theory, whereas the substrate-structure interaction is founded on the Winkler-foundation model. The governing differential equilibrium equation (GDEE) and its corresponding boundary conditions for the local beam model on the elastic substrate medium, considering the surface effect, are obtained using the principle of virtual displacement. Then, the stress-driven mixture of integral elasticity is used to extend the GDEE and its relevant boundary conditions from the local beam-substrate medium model to the nonlocal beam-substrate medium model. All the calculations for this work are performed on the computer software Mathematica [77], and all materials in this work are stated on the assumption that they are linearly homogenous and isotropic materials. From all of the above, the research methodology of this work is summarized in Fig. 1, including the processes of mathematical modeling and simulation, respectively. The details of the model formulation can be expressed as follows:

2.1. Kinematics of Euler-Bernoulli beam theory

In this work, the Euler-Bernoulli beam theory [78] is used to describe the kinematic configuration of the beam, simplifying the beam-substrate medium formulation. According to this theory, it is considered that the plane sections are at exactly parallel to the neutral axis prior to any deformation. Following deformation, the plane sections remain within the same plane and perpendicular to the neutral axis. Consequently, the movement of a generic point along the x-, y-, and z-axes can be expressed as [11]:

$$U_x(x,y) = -y\frac{dv(x)}{dx};\;\; U_y(x,y) = v(x);\;\; \text{and}\;\; U_z(x,y) = 0 \tag{1}$$

where y denotes the distance from the reference axis x to the generic point; $v(x)$ denotes the transverse displacement field; and $U_x(x,y)$, $U_y(x,y)$, and $U_z(x,y)$ denote the displacement fields along the x-, y-, and z-axes, respectively.

Based on the assumption of small deformation, the axial strain $\varepsilon_{xx}(x)$ for the planer Euler-Bernoulli beam system is given as [78]:

$$\varepsilon_{xx}(x) = \frac{dU_x(x,y)}{dx} = -y\frac{d^2v(x)}{dx^2} = -y\kappa(x) \tag{2}$$

where $\varepsilon_{xx}(x)$ denotes the beam axis strain and is the complementary conjugate-work pair of axial stress $\sigma_{xx}(x)$; and $\kappa(x) = d^2v(x)/dx^2$ denotes the nanobeam bending curvature.

2.2. Substrate medium model

In this study, the idea of the Winkler foundation [48, 74] is employed to model the interaction between the substrate medium and the nanobeam. According to the basis of this foundational model [48, 74], a transversely tangential spring is attached throughout the length of the beam to duplicate the surrounding substrate media, as depicted in Fig. 2. Therefore, the relationship between the substrate medium's properties can be expressed as [48]:

$$D_{sub}(x) = k_{sub}\Delta_{sub}(x) \tag{3}$$

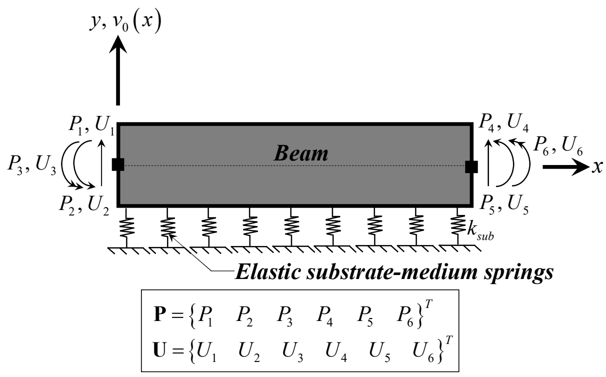

Fig. 2. Mathematical nonlocal beam model resting on the elastic substrate medium.

where k_{sub} denotes the elastic modulus's substrate medium; $D_{sub}(x)$ denotes the substrate medium interactive force and is the conjugate-work pair of the substrate deformation $\Delta_{sub}(x)$.

Sae-Long et al. [48] stated that the substrate deformation of the transversely tangential spring, based on the Winkler-foundation model, is considered to be fully compatible with the beam deformation. Therefore, the connection between the deformation of the substrate $\Delta_{sub}(x)$ and the transverse displacement $v(x)$ of the beam can be expressed as [48]:

$$\Delta_{sub}(x) = v(x) \tag{4}$$

By enforcing the compatibility relation of Eq. (4), the substrate medium's constitutive relation of Eq. (3) can be rewritten in term of $v(x)$ as [48]:

$$D_{sub}(x) = k_{sub}v(x) \tag{5}$$

2.3. Surface-energy continuum model

Experiments and simulations [61-68] show that there is a difference in the energy of the relevant atom between the bulk and free surface of the material as the structure's dimensions approach the nanoscale. This phenomenon is referred to as the "*surface-energy*" effect. It is a size-dependent impact that happens in micro- and nanostructures. It is crucial to include this effect when analyzing the properties of these structures. Several studies [9, 11, 18, 19, 28, 32, 48, 64-68] have highlighted the significance of this effect. The current study utilizes the surface-energy continuum model developed by Gurtin and Murdoch [61-62] to incorporate the influence of surface energy in the nanobeam system. Figure 3 illustrates that the beam section consists of a central core and an outer layer that wraps around it. The connection between the main core and the outside layer is seen as fully established, and the thickness of the outer layer is treated as a theoretically negligible layer, following Cammarata's surface theory [63]. Hence, the correlation between surface stress and surface strain results in [11]:

$$\tau_{pq}^{sur} = \left[\tau_{res}^{sur} + \left(\lambda_0^{sur} + \mu_0^{sur}\right)u_{\gamma,\gamma}^{sur}\right]\delta_{pq} + \mu_0^{sur}\left(u_{p,q}^{sur} + u_{q,p}^{sur}\right) - \tau_{res}^{sur}u_{q,p}^{sur} \tag{6}$$

$$\tau_{np}^{sur} = \tau_{res}^{sur}u_{n,p}^{sur} \tag{7}$$

where τ_{pq}^{sur} and τ_{np}^{sur} are the surface stresses in and out of plane, respectively; τ_{res}^{sur} is the residual surface stress produced from the atomistic simulation under unconstrained conditions [79]; λ_0^{sur} and μ_0^{sur} denote the surface elastic constants; p and q are the nanobeam's Cartesian coordinates in the plane of the lateral surface; and u^{sur} denotes the surface-layer deformation.

Limkatanyu et al. [11] provided the expression for the non-zero component of in-plane and out-of-plane surface stress in the planar Euler-Bernoulli beam system, based on the surface constitutive relations given by Eqs. (6) and (7), one has:

$$\tau_{xx}^{sur}(x) - \tau_{res}^{sur} = E_{xx}^{sur}\varepsilon_{xx}^{sur}(x) \tag{8}$$

$$\tau_{nx}^{sur}(x) = \tau_{res}^{sur}\varepsilon_{nx}^{sur}(x) \tag{9}$$

where $E_{xx}^{sur} = \lambda_0^{sur} + 2\mu_0^{sur}$ denotes the elastic modulus; $\tau_{xx}^{sur}(x)$ denotes the surface stress in plane and is the conjugate-work pair of the surface strain in plane $\varepsilon_{xx}^{sur}(x)$; and $\tau_{nx}^{sur}(x)$ denotes the surface stress out of plane and is the conjugate-work pair of the surface strain out of plane $\varepsilon_{nx}^{sur}(x)$.

Based on the kinematic configuration of Euler-Bernoulli beam theory as presented in Eqs. (1) and (2), the outer surface layer, as shown in Fig. 3, is assumed to be fully compatible with the nanobeam cross-section. Following this assumption, the compatibility relations between the surface deformations and the beam deformation are [11]:

$$\varepsilon_{xx}^{sur}(x) = \varepsilon_{xx}(x) = -y\frac{d^2v(x)}{dx^2} \tag{10}$$

$$\varepsilon_{nx}^{sur}(x) = n_y\frac{dv(x)}{dx} \tag{11}$$

where n_y denotes the y-axis unit vector normal to the beam-section lateral surface.

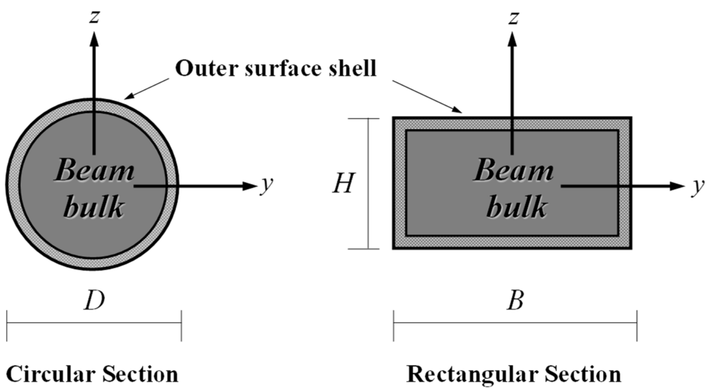

Fig. 3. Circular and rectangular cross-sections of beam bulk with the inclusion of the surface-energy effect [9, 11].

The representation of surface stresses in both the in-plane and out-of-plane directions can be achieved by including the surface compatibility relations from Eqs. (10) and (11) into the surface constitutive relations from Eqs. (8) and (9) in the following manner [11]:

$$\tau_{xx}^{sur}(x) - \tau_{res}^{sur} = -yE_{xx}^{sur}\frac{d^2\upsilon(x)}{dx^2} \tag{12}$$

$$\tau_{nx}^{sur}(x) = n_y\tau_{res}^{sur}\frac{d\upsilon(x)}{dx} \tag{13}$$

2.4. Local beam-substrate system with the inclusion of surface-energy effect

2.4.1. Equilibrium

The notion of virtual displacement is invoked to establish the GDEE and its associated boundary conditions for the local beam-substrate system incorporating the surface-energy effect. The conventional manifestation of the virtual displacement principle is:

$$\delta W = \delta W_{\text{int}} + \delta W_{\text{ext}} = 0 \tag{14}$$

where δW_{int} denotes the system internal virtual work; δW_{ext} denotes the system external virtual work; and δW denotes the system total virtual work.

The values of δW_{int} and δW_{ext} for the local beam-substrate system, taking into account the surface-energy impact, can be expressed using the virtual displacement principle stated in Eq. (14) as:

$$\delta W_{\text{int}} = \underbrace{\int_L\left(\int_A \sigma_{xx}(x)dA\right)\delta\varepsilon_{xx}(x)dx}_{\text{Beam contribution}} + \underbrace{\int_L D_{sub}(x)\delta\Delta_{sub}(x)dx}_{\text{Substrate medium contribution}} + \underbrace{\overbrace{\int_L\left(\oint_\Gamma\left(\tau_{xx}^{sur}(x)-\tau_{res}^{sur}\right)\delta\varepsilon_{xx}^{sur}(x)d\Gamma\right)dx}^{\text{In-plane component}} + \overbrace{\int_L\left(\oint_\Gamma \tau_{nx}^{sur}(x)\delta\varepsilon_{nx}^{sur}(x)d\Gamma\right)dx}^{\text{Out-of-plane component}}}_{\text{Surface-energy contribution}} \tag{15}$$

$$\delta W_{\text{ext}} = -\underbrace{\int_L w_y(x)dx}_{\text{External load contribution}} - \underbrace{\delta\mathbf{U}^T\mathbf{P}}_{\text{Boundary terms}} \tag{16}$$

where A denotes the beam-section area; Γ denotes the beam-section perimeter; $w_y(x)$ denotes the external transverse load; $\mathbf{U} = [U_1 \;\; U_2 \;\; U_3 \;\; U_4 \;\; U_5 \;\; U_6]^T$ denotes the displacement vector containing the end nodal displacements; and $\mathbf{P} = [P_1 \;\; P_2 \;\; P_3 \;\; P_4 \;\; P_5 \;\; P_6]^T$ denotes the force vector containing the end nodal forces. It is worthy to note that the force vector $\mathbf{P}$ is the conjugate-work pair of the displacement vector $\mathbf{U}$, as illustrated in Fig. 2.

The internal virtual work of the system δW_{int} in Eq. (15) can be expressed in terms of the virtual transverse displacement $\upsilon(x)$ by using the compatibility relations of Eqs. (2), (4), (10), and (11) as follows:

$$\delta W_{\text{int}} = \int_L M^B(x)\frac{d^2\delta\upsilon(x)}{dx^2}dx + \int_L D_{sub}(x)\delta\upsilon(x)dx + \int_L M^{sur}(x)\frac{d^2\delta\upsilon(x)}{dx^2}dx + \int_L V^{sur}(x)\frac{d\delta\upsilon(x)}{dx}dx \tag{17}$$

where $M^B(x) = -\int_A y\sigma_{xx}(x)dA$ denotes the beam-section bending moment; $V^{sur}(x) = \oint_\Gamma n_y\tau_{nx}^{sur}(x)d\Gamma$ denotes the surface-induced shear force distribution; and $M^{sur}(x) = -\oint_\Gamma y\left(\tau_{xx}^{sur}(x) - \tau_{res}^{sur}\right)d\Gamma$ denotes the surface-induced bending moment distribution.

Based on the surface constitutive relations of Eqs. (12) and (13), the surface-induced bending moment distribution $M^{sur}(x)$ and the surface-induced shear force distribution $V^{sur}(x)$ as illustrated in Eq. (17) can be written in term of $\upsilon(x)$ as follows:

$$M^{sur}(x) = E_{xx}^{sur}I_\Gamma\frac{d^2\upsilon(x)}{dx^2} \tag{18}$$

$$V^{sur}(x) = \tau_{res}^{sur}S_\Gamma\frac{d\upsilon(x)}{dx} \tag{19}$$

where $I_\Gamma = \oint_\Gamma y^2dA$ denotes the second moment perimeter; and $S_\Gamma = \oint_\Gamma n_y^2d\Gamma$.

By replacing the internal virtual work δW_{int} of the system from Eq. (17) and the external virtual work δW_{ext} of the system from Eq. (16) in the Eq. (14) for the total virtual work of the system δW, the expression for the total virtual work of the system can be rephrased as:

$$\delta W = \int_L M(x)\frac{d^2\delta\upsilon(x)}{dx^2}dx + \int_L D_{sub}(x)\delta\upsilon(x)dx + \int_L V^{sur}(x)\frac{d\delta\upsilon(x)}{dx}dx - \int_L w_y(x)dx - \delta\mathbf{U}^T\mathbf{P} = 0 \tag{20}$$

where $M(x) = M^B(x) + M^{sur}(x)$ denotes the sectional bending moment with the inclusion of the surface-induced bending moment distribution.

The technique of integration by parts is utilized in Eq. (20) to transform the differential operators from the virtual transverse displacement $\delta\upsilon(x)$ to the sectional forces, yielding the subsequent expression:

$$\delta W = \int_L \delta\upsilon(x)\left[\frac{d^2M(x)}{dx^2} - \frac{dV^{sur}(x)}{dx} + D_{sub}(x) - w_y(x)\right]dx + \delta\upsilon(x)\left[-\frac{dM(x)}{dx} + V^{sur}(x)\right]_{x=0}^{x=L} + \frac{d\delta\upsilon(x)}{dx}\left[M(x)\right]_{x=0}^{x=L} - \delta\mathbf{U}^T\mathbf{P} = 0 \tag{21}$$

The GDEE of the local beam-substrate system, taking into consideration the surface-energy impact, is derived by considering the variability of parameter $\delta\upsilon(x)$ in Eq. (21), leading to the following expression:

$$\frac{d^2M(x)}{dx^2}-\frac{dV^{sur}(x)}{dx}+D_{sub}(x)-w_y(x) \tag{22}$$

Applying the Cartesian sign convention and considering the arbitrary value of $\delta\upsilon(x)$ in Eq. (21), the boundary conditions for the local beam-substrate system with the surface-energy effect are as follows:

$$\begin{aligned}&P_1=-\left[-\frac{dM(x)}{dx}+V^{sur}(x)\right]_{x=0};\ P_2=-\left[M(x)\right]_{x=0};\\&P_3=\left[-\frac{dM(x)}{dx}+V^{sur}(x)\right]_{x=L};\ P_4=\left[M(x)\right]_{x=L};\end{aligned} \tag{23}$$

2.4.2. Stress-driven mixture of integral elasticity

In this study, the nonlocality within the micro- and nanostructures is represented based on the mixture stress-driven elasticity model as proposed by Barretta et al. [80]. The total strain $\varepsilon_{xx}(x)$ at the generic point is defined as a function of the stress at all neighboring points. Therefore, the constitutive relation for the isotropic homogeneous structures in the one-dimension Euler-Bernoulli nanobeam problem is given by Vaccaro et al. [54] as:

$$\varepsilon_{xx}(x)=\frac{1}{E_{xx}}\left[\alpha\sigma(x)+(1-\alpha)\int_L\Omega_{L_c}(x,\xi)\sigma(x)d\xi\right] \tag{24}$$

where E_{xx} is the elastic modulus of the nanobeam; $\Omega_{L_c}(x,\xi)$ defines an averaging kernel function, which is associated with the material length-scale parameter L_c; and α represents the mixture parameter, which is defined in the range of $0\le\alpha\le1$. It is worth emphasizing that the purely nonlocal stress-driven integral model is obtained when the mixture parameter is equal to 0 $(\alpha=0)$. Furthermore, when the mixture parameter reaches 1 $(\alpha=1)$, the local constitutive of elasticity theory is obtained [54].

For the planer Euler-Bernoulli beam system, the total strain $\varepsilon_{xx}(x)$ in Eq. (24) can be expressed in term of the flexural nanobeam curvature $\kappa(x)$ based on the compatibility equation of Eq. (2) by assuming the flexural nanobeam curvature $\kappa(x)$ to be coincident with the elastic bending curvature [54]. So, the flexural nanobeam curvature for the nanobeam system with the inclusion of the surface-energy effect can be expressed as the integral convolution among the bending moment $M(x)$, constant effective flexural rigidity $(EI)_{eff}^{BS}$, and kernel function $\Omega_{L_c}(x,\xi)$ as [54]:

$$\kappa(x)=\alpha\frac{M(x)}{(EI)_{eff}^{BS}}+(1-\alpha)\int_L\Omega_{L_c}(x,\xi)\frac{M(\xi)}{(EI)_{eff}^{BS}}d\xi \tag{25}$$

where $(EI)_{eff}^{BS}=E_{xx}I+E_{xx}^{sur}I_\Gamma$ denotes the nanobeam's flexural rigidity with the surface-energy effect; and I represents the nanobeam's moment inertia.

As suggested by Vaccaro et al. [54], the bi-exponential function (Helmholtz's kernel) is selected herein to describe the effect of nonlocality:

$$\Omega_{L_c}(x)=\frac{1}{2L_c}\exp\left(-\frac{|x|}{L_c}\right) \tag{26}$$

where $L_c=e_0a$ defines the material length-scale parameter; e_0 denotes the material constant; and a is the internal characteristic length. It is important to note that the bi-exponential function in Eq. (26) satisfies Eringen's conditions of symmetry, positivity, and limited impulsivity [58].

Substituting the kernel function of Eq. (26) into Eq. (25) and applying the differential operator, the equivalent differential equation and its associated constitutive boundary conditions are given by Vaccaro et al. [54] as follows:

- Equivalent differential equation:

$$\frac{\kappa(x)}{L_c^2}-\frac{d^2\kappa(x)}{dx^2}=\frac{1}{(EI)_{eff}^{BS}}\left[\frac{M(x)}{L_c^2}-\alpha\frac{d^2M(x)}{dx^2}\right] \tag{27}$$

- Constitutive boundary conditions:

$$\left[\frac{d\kappa(x)}{dx}-\frac{\kappa(x)}{L_c}=\frac{\alpha}{(EI)_{eff}^{BS}}\left(\frac{dM(x)}{dx}-\frac{M(x)}{L_c}\right)\right]_{x=0}\ \text{and}\ \left[\frac{d\kappa(x)}{dx}+\frac{\kappa(x)}{L_c}=\frac{\alpha}{(EI)_{eff}^{BS}}\left(\frac{dM(x)}{dx}+\frac{M(x)}{L_c}\right)\right]_{x=L} \tag{28}$$

2.5. Nonlocal beam-substrate system with the inclusion of surface-energy effect

2.5.1. Equilibrium

By enforcing the system equilibrium equation of Eq. (22) in term of the second derivative of the bending moment $d^2M(x)/dx^2=dV^{sur}(x)/dx-D_{sub}(x)+w_y(x)$ and then substituting into the equivalent differential equation of Eq. (27), the result leads to the following expression:

$$M(x)=(EI)_{eff}^{BS}\kappa(x)-L_c^2(EI)_{eff}^{BS}\frac{d^2\kappa(x)}{dx^2}+\alpha L_c^2\left[\frac{dV^{sur}(x)}{dx}-D_{sub}(x)+w_y(x)\right] \tag{29}$$

Employing the compatibility relation of Eq. (2) and using the constitutive relations of Eqs. (5), (18), and (19), the sectional bending moment $M(x)$ in Eq. (29) can be rewritten as:

$$M(x) = -(EI)_{eff}^{H}\frac{d^4 v(x)}{dx^4} + (EI)_{eff}^{L}\frac{d^2 v(x)}{dx^2} - \alpha L_c^2 k_{sub} v(x) + \alpha L_c^2 w_y(x) \tag{30}$$

where $(EI)_{eff}^{H} = L_c^2 (EI)_{eff}^{BS}$ denotes the higher-order flexural stiffness; and $(EI)_{eff}^{L} = (EI)_{eff}^{BS} + \alpha L_c^2 \tau_{res}^{sur} S_\Gamma$ defines the lower-order flexural stiffness.

By differentiating twice the relation in Eq. (30) by the spatial variable x and then substituting this relation into the equilibrium relation in Eq. (22), the GDEE of the nonlocal nanobeam model on the substrate medium with the inclusion of the surface-energy effect yields:

$$-(EI)_{eff}^{H}\frac{d^6 v(x)}{dx^6} + (EI)_{eff}^{L}\frac{d^4 v(x)}{dx^4} - (K)_{eff}^{H}\frac{d^2 v(x)}{dx^2} + k_{sub} v(x) - w_y(x) + \alpha L_c^2 \frac{d^2 w_y(x)}{dx^2} = 0 \tag{31}$$

where $(K)_{eff}^{H} = \tau_{res}^{sur} S_\Gamma + \alpha L_c^2 k_{sub}$ represents the lower-order flexural rigidity. It is observed from Eq. (31) that this equation is the core of the proposed model to obtain the solution of $v(x)$. Both higher-order term (6th-order) and lower-order terms (4th-order and 2th-order), induced by the nonlocality and surface-energy effect, play an essential role in the flexural rigidity to resist bending behaviors. Furthermore, this equation can degenerate to the form of the governing differential equation of the local beam model on Winkler foundation when all variables relevant to the nonlocality and surface-energy effects are suppressed $(L_c = E_{xx}^{sur} = \tau_{res}^{sur} = 0)$ [81].

Similarly, the classical boundary conditions of Eq. (23) can be rewritten based on the constitutive relations of Eqs. (18) and (19) and the bending moment of Eq. (30). This leads to the following expression:

$$\begin{aligned}
P_1 &= -\left[\underbrace{(EI)_{eff}^{H}\frac{d^5 v(x)}{dx^5} - (EI)_{eff}^{L}\frac{d^3 v(x)}{dx^3} + (K)_{eff}^{H}\frac{dv(x)}{dx} - \alpha L_c^2 \frac{dw_y(x)}{dx}}_{V(0)}\right]_{x=0} ; \\
P_2 &= -\left[\underbrace{-(EI)_{eff}^{H}\frac{d^4 v(x)}{dx^4} + (EI)_{eff}^{L}\frac{d^2 v(x)}{dx^2} - \alpha L_c^2 k_{sub} v(x) + \alpha L_c^2 w_y(x)}_{M(0)}\right]_{x=0} ; \\
P_3 &= \left[\underbrace{(EI)_{eff}^{H}\frac{d^5 v(x)}{dx^5} - (EI)_{eff}^{L}\frac{d^3 v(x)}{dx^3} + (K)_{eff}^{H}\frac{dv(x)}{dx} - \alpha L_c^2 \frac{dw_y(x)}{dx}}_{V(L)}\right]_{x=L} ; \\
P_4 &= \left[\underbrace{-(EI)_{eff}^{H}\frac{d^4 v(x)}{dx^4} + (EI)_{eff}^{L}\frac{d^2 v(x)}{dx^2} - \alpha L_c^2 k_{sub} v(x) + \alpha L_c^2 w_y(x)}_{M(L)}\right]_{x=L}
\end{aligned} \tag{32}$$

Based on the relation in Eq. (30), the constitutive boundary conditions of Eq. (28) can be rewritten as:

$$\begin{aligned}
&\left[\begin{aligned}&\frac{\alpha (EI)_{eff}^{H}}{(EI)_{eff}^{BS}}\frac{d^5 v(x)}{dx^5} - \frac{\alpha (EI)_{eff}^{H}}{L_c (EI)_{eff}^{BS}}\frac{d^4 v(x)}{dx^4} + \left(1 - \frac{\alpha (EI)_{eff}^{L}}{(EI)_{eff}^{BS}}\right)\frac{d^3 v(x)}{dx^3} - \left(\frac{1}{L_c} - \frac{\alpha (EI)_{eff}^{L}}{L_c (EI)_{eff}^{BS}}\right)\frac{d^2 v(x)}{dx^2} \\ &+ \frac{\alpha^2 L_c^2 k_{sub}}{(EI)_{eff}^{BS}}\frac{dv(x)}{dx} - \frac{\alpha^2 L_c k_{sub}}{(EI)_{eff}^{BS}} v(x) + \frac{\alpha^2 L_c w_y(x)}{(EI)_{eff}^{BS}} - \frac{\alpha^2 L_c^2}{(EI)_{eff}^{BS}}\frac{dw_y(x)}{dx} = 0\end{aligned}\right]_{x=0} ; \\
&\left[\begin{aligned}&\frac{\alpha (EI)_{eff}^{H}}{(EI)_{eff}^{BS}}\frac{d^5 v(x)}{dx^5} + \frac{\alpha (EI)_{eff}^{H}}{L_c (EI)_{eff}^{BS}}\frac{d^4 v(x)}{dx^4} + \left(1 - \frac{\alpha (EI)_{eff}^{L}}{(EI)_{eff}^{BS}}\right)\frac{d^3 v(x)}{dx^3} + \left(\frac{1}{L_c} - \frac{\alpha (EI)_{eff}^{L}}{L_c (EI)_{eff}^{BS}}\right)\frac{d^2 v(x)}{dx^2} \\ &+ \frac{\alpha^2 L_c^2 k_{sub}}{(EI)_{eff}^{BS}}\frac{dv(x)}{dx} + \frac{\alpha^2 L_c k_{sub}}{(EI)_{eff}^{BS}} v(x) - \frac{\alpha^2 L_c w_y(x)}{(EI)_{eff}^{BS}} - \frac{\alpha^2 L_c^2}{(EI)_{eff}^{BS}}\frac{dw_y(x)}{dx} = 0\end{aligned}\right]_{x=L}
\end{aligned} \tag{33}$$

2.5.2. Analytical solution for static bending analysis

The general solution of Eq. (31) can be divided into two parts, namely the homogeneous part and the particular part. Thus, the general solution for the static bending analysis of the present nonlocal nanobeam on the elastic substrate medium can be expressed as follows:

$$v(x) = v_h(x) + v_p(x) \tag{34}$$

where $v_h(x)$ is the part of the homogeneous solution for $w_y(x) = 0$; and $v_p(x)$ is the part of the particular solution for $w_y(x) \neq 0$. It is interesting to observe that the form of the differential equation in Eq. (31) is similar to the general form of the governing differential equation of the beam system on a three-parameter foundation, as proposed by Morfidis [82] and Avramidis and Morfidis [83]. Therefore, the general solutions of the beam system on the three-parameter foundation can be applied herein, resulting in the homogenous solution $v_h(x)$ of Eq. (34) as follows:

$$v_h(x) = \gamma_1(x)C_1 + \gamma_2(x)C_2 + \gamma_3(x)C_3 + \gamma_4(x)C_4 + \gamma_5(x)C_5 + \gamma_6(x)C_6 \tag{35}$$

where C_1, C_2, C_3, C_4, C_5, and C_6 are the generalized coordinates derived based on the boundary constraints; and $\gamma_1(x)$, $\gamma_2(x)$, $\gamma_3(x)$, $\gamma_4(x)$, $\gamma_5(x)$, and $\gamma_6(x)$ are the basic displacement functions presented in Appendix A.

3. Results and Discussion

The results of this study are presented through numerical examples based on the computer software Mathematica [77]. In this section, four numerical simulations are employed to present the impact of the mixture parameter on the static bending analysis of nanobeam systems. The first simulation verifies the proposed mixture stress-driven nonlocal beam model with the experiment and shows the influence of the mixture parameter on the cantilever nanobeam system. The second investigates the effects of surface-energy and substrate-structure interaction on nanobeam deflection. The third and fourth simulations investigate how system variable variation affects the normalized beam deflection and effective bulk Young's modulus (EBYM) of nanobeam systems on elastic substrate media.

3.1. Example I: model verification

As demonstrated in the literature [11, 46-49], several nonlocal beam models fail to predict the small-scale effect within the micro- and nano-scale beam problems, especially the cantilever beam problem subjected to a transverse point load at the free-end boundary. Furthermore, many nonlocal beam models have not been verified with experiments. As a result, the primary goal of this simulation is to validate the mixture stress-driven nonlocal beam model with the experiment and to demonstrate the influence of the mixture parameter on the bending analysis of the cantilever nanobeam system. The experimental test of the silicon microcantilever beam subjected to the free-end transverse point load P_{end}, was conducted by Tang and Alici [15], is selected to be employed herein. The elastic modulus E_{xx} of silicon is 169 GPa, while the beam dimension is 35x2 μm^2, as shown in Fig. 4. The beam's length is 130 μm, and the material length scale parameter follows those suggested by Darban et al. [10] with L_c = 78 μm. The mixture parameter varied from 0 to 1 $(0 \le \alpha \le 1)$ to investigate the impact of the nonlocal phase on the nanobeam system. In this simulation, two nonlocal beam models are employed to be compared, namely: (a) the proposed nonlocal beam model and (b) the simplified strain-gradient beam model of Sae-Long et al. [48].

Figure 5 presents the load-displacement diagram at the free end of the silicon microcantilever beam obtained from the analytical beam models compared to the experiment. The experimental result data, as presented by the circle markers, was employed to represent the benchmark response and was conducted based on Darban et al.'s work [10], which was established from the experiment of Tang and Alici [15].

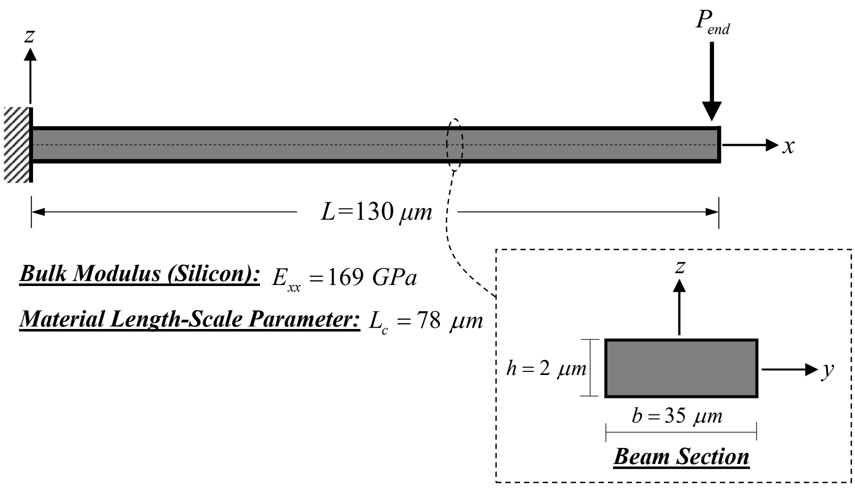

Fig. 4. Simulation I: model verification.

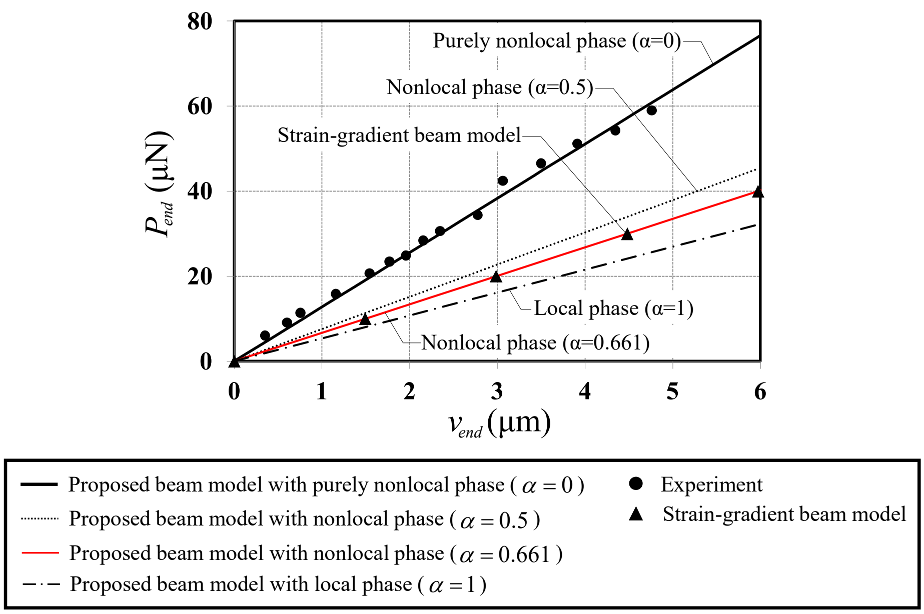

Fig. 5. Load-displacement relation at free-end boundary of Simulation I.

In analytical procedure, the proposed model's response is obtained based on the complete suppression of substrate-structure interaction and surface-energy effect ($k_{sub} = E_{xx}^{sur} = \tau_{res}^{sur} = 0$). The result discloses that the response of the proposed nanobeam model well matches the result obtained from the experiment in the case of the purely nonlocal phase ($\alpha = 0$). This match is identically observed in the nonlocal stress-driven beam model of Darban et al. [10] since the vanishing of the elastic constitutive term in Eq. (25) leads to the constitutive law of the stress-driven nonlocal elasticity theory, as proposed by Romano and Barretta [84]. Furthermore, it can be seen that the stiffness of the beam system decreases with the increasing value of the mixture parameter until one ($\alpha = 1$). The local beam model's response will be recovered, as illustrated in Fig. 5. This softening phenomenon is similar to that found in the mixed two-phase stress-driven nonlocal beam model of Behdad and Arefi [56]. Subsequently, it is interesting to observe that the load-displacement response of the simplified strain-gradient beam model [48] is a subset of that obtained from the proposed mixture two-phase nonlocal beam model when the mixture parameter is approximately about $\alpha = 0.661$ in this particular case.

3.2. Example II: effects of surface-energy and substrate-structure interaction

To demonstrate the effects of surface energy and substrate-structure interaction on the bending characteristics of nanobeam systems, a lead cantilever nanobeam system with or without an elastic substrate medium, as shown in Fig. 6, is employed in this study. The nanobeam is subjected to a free-end point load of P_{end} = 10 nN, and its material properties are provided by Cuenot et al. [85] and Wan et al. [86], including a bulk modulus E_{xx} of 16 GPa, a surface elastic modulus E_{xx}^{sur} of 8 nN/nm, and a residual surface stress τ_{res}^{sur} of 0.63 nN/nm. The geometric properties of the nanobeam follow those used by Limkatanyu et al. [11, 28], such as a length L of 1,000 nm with a 50×100 nm^2 rectangular cross-section, as shown in Fig. 6. The mixture parameter is set to a purely nonlocal phase ($\alpha = 0$), while the material length scale parameter L_c is kept constant at 100 nm. The substrate-stiffness parameter follows those used by Limkatanyu et al. [18] with K_s of 0.095 nN/nm^3 and $k_s = K_s b$ of 0.475 nN/nm^2. In this simulation, four analytical models are employed to be compared, namely: (a) the nonlocal stress-driven beam model without the surface-energy effect [54]; (b) the nonlocal stress-driven beam model with the surface-energy effect; (c) the nonlocal stress-driven beam-substrate medium model without the surface-energy effect; and (d) the nonlocal stress-driven beam-substrate medium model with the surface-energy effect.

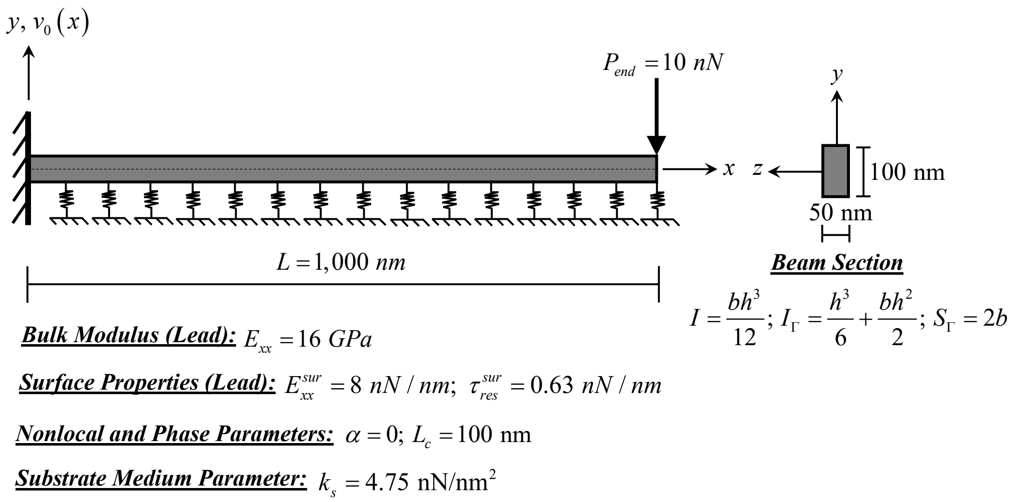

Fig. 6. Simulation II: Effects of surface-energy and substrate-structure interaction.

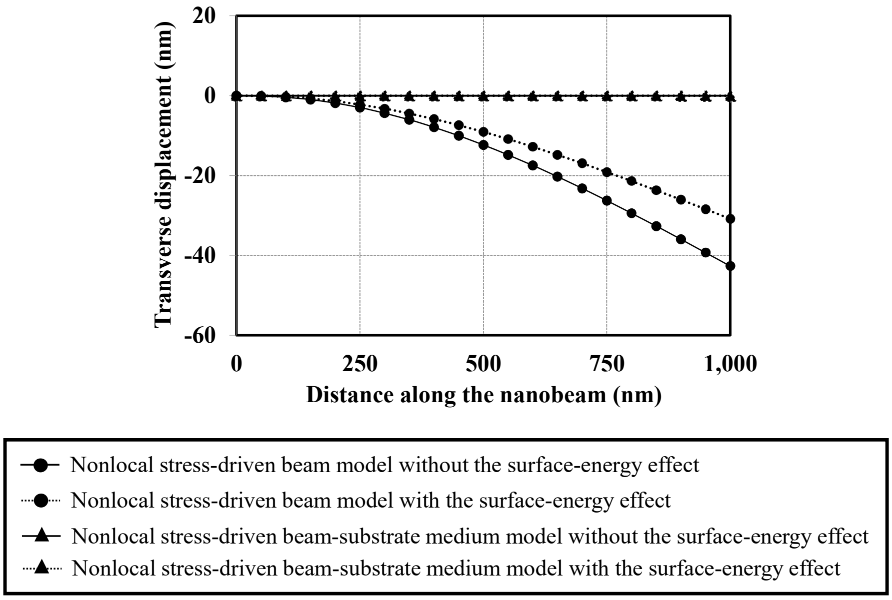

Fig. 7. Transverse displacement versus distance along the nanobeam of Simulation II.

Figure 7 presents the analytical transverse displacement along the nanobeam length obtained from four analytical models. The effect of surface energy is evident in this diagram for the nonlocal beam models. This effect leads to an increase in system stiffness and a decrease in the end transverse displacement by approximately 27.71% in this particular case. In addition to the influence of surface energy, the substrate-structure interaction further enhances system stiffness. This is evident when comparing the nonlocal beam model and the nonlocal beam-substrate medium model without the surface effect. The end transverse displacement decreases by about 99.90% for the model with the elastic substrate medium. However, the stiffening effect caused by surface energy on the nanobeam deflection is reduced when substrate-structure interaction is considered, resulting in a reduction of the transverse displacement by about 1.23%. This result highlights the impact of surface energy and substrate-structure interaction on the analysis of the static response of nanoscale structures.

3.3. Example III: parametric study of system parameters on the beam deflection

It can be observed in simulation I that the bending behavior of nanobeam is influenced by the variation of the mixture parameter. Thus, this simulation provides a set of varied system parameters to examine the impact of these parameters on the beam deflection for the nanobeam-substrate system. The lead cantilever nanobeam on the elastic substrate medium subjected to a free-end point load of P_{end} = 10 nN is employed to study in this simulation. The nanobeam material properties are similar to those used in Simulation II and are given by Cuenot et al. [85] and Wan et al. [86], such as a bulk modulus E_{xx} of 16 GPa, a surface elastic modulus E_{xx}^{sur} of 8 nN/nm, and a residual surface stress τ_{res}^{sur} of 0.63 nN/nm, respectively. The geometric properties of nanobeam follow those used by Limkatanyu et al. [11, 28], such as nanobeam's length L of 1,000 nm with a 100x100 nm^2 square cross-section as shown in Fig. 8. The system parameters investigated herein include the mixture parameter α with a range of $0 \le \alpha \le 1$, the normalized material length scale parameter $\xi_c = L_c / L$ with a range of $0 \le \xi_c \le 0.2$, and the non-dimensional substrate-stiffness parameter $\bar{K}_{sub}$ with a range of $1 \le \bar{K}_{sub} \le 10$. The non-dimensional substrate-stiffness parameter $\bar{K}_{sub}$ is used to vary the value of a substrate medium modulus k_{sub} and is defined by the suggestion of Limkatanyu et al. [11] as follows:

$$\bar{K}_{sub} = \frac{k_{sub} L^4}{E_{xx} I} \tag{36}$$

Figure 9 demonstrates the variation of the normalized beam deflection $\upsilon_{nor} = \upsilon_{\text{Proposed}} / \upsilon_{\text{Classical}}$ at the free end of the nanobeam with the variation of the mixture parameter α, the normalized material length scale parameter ξ_c, and the non-dimensional substrate-stiffness parameter $\bar{K}_{sub}$. Based on the system parameters, only the solution of Case I $(\Delta = \eta^3 + \Xi^2 > 0)$ is activated for this case study. The diagram in Fig. 9 clearly shows that the influence of nonlocality grows as the nonlocal phase approaches the purely nonlocal phase (decreasing of the mixture parameter α). Similarly, as the material length scale parameter L_c is increased, the nonlocality increases. However, this stiffening phenomenon will degrade when the substrate medium is stiffened (with an increase in the non-dimensional substrate-stiffness parameter $\bar{K}_{sub}$), as seen at point A.

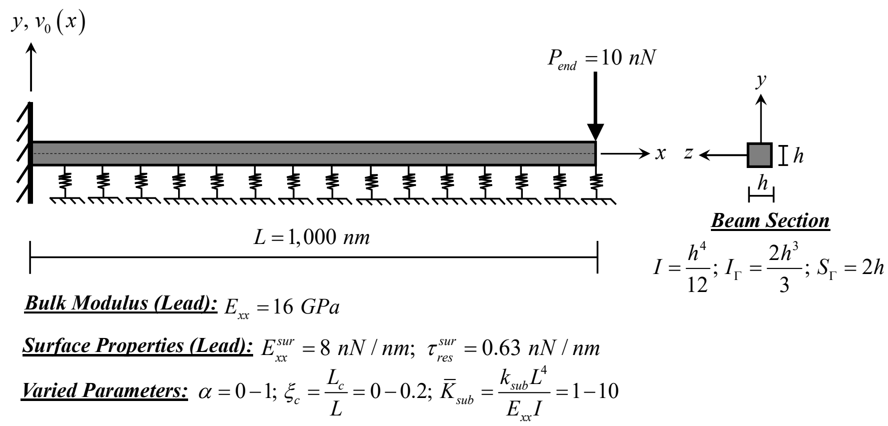

Fig. 8. Simulation III: Parametric study of system parameters on the beam deflection.

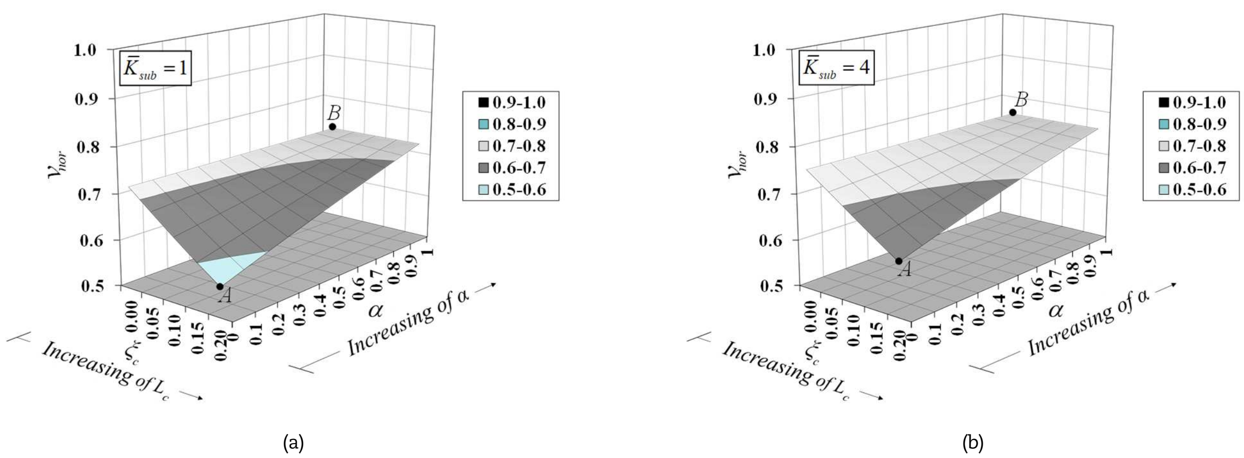

Fig. 9. Variation of normalized beam deflection υ_{nor} with variation on mixture parameter α, normalized material length scale parameter ξ_c and non-dimensional substrate-stiffness parameter: (a) $\bar{K}_{sub} = 1$; (b) $\bar{K}_{sub} = 4$; (c) $\bar{K}_{sub} = 7$; and (d) $\bar{K}_{sub} = 10$.

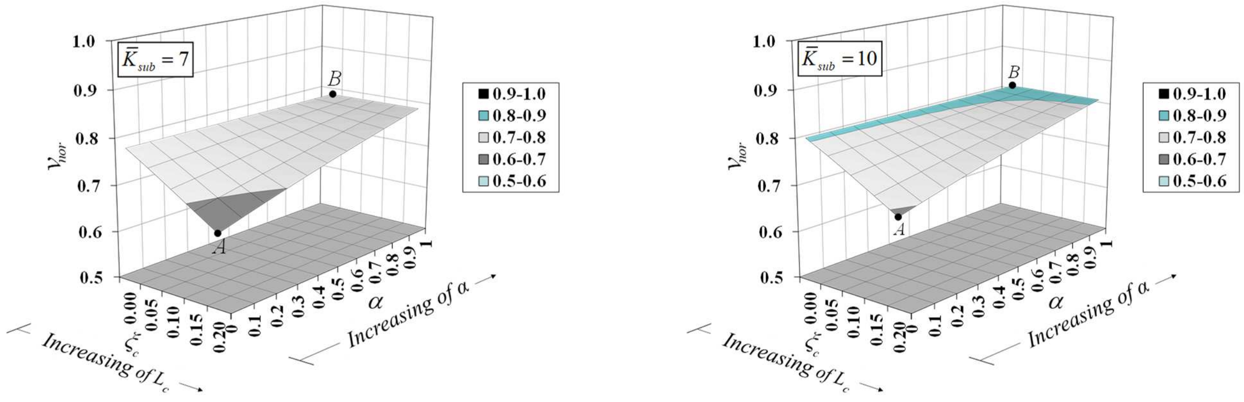

(c) (d)

Fig. 9. Continued.

Furthermore, as the nonlocal phase approaches the local phase $(\alpha \to 0$ or $\xi_c = 0)$, the beam deflection of the proposed model reaches the beam response obtained from the local beam model, as shown at Point B. In addition to the nonlocal effect, the surface-energy effect leads to the stiffening phenomenon as well as the nonlocality, but it is independent on the nonlocal parameters (α and L_c) and a constantly enhanced system stiffness due to a constant of the beam surface-area/section-area ratio (A_S / A_B) for this particular case. This can be observed at Point B, where the enhancement of system stiffness caused by the surface-energy will decrease when the substrate medium becomes stiffer.

From the observed results in this simulation, it can be inferred that the nonlocality driven by the mixture parameter α and material length scale parameter L_c, the surface-energy, and the substrate-structure interaction have an essential impact on the static bending analysis of the nanobeam system on the substrate medium. These influences result in increased stiffness of the system within the micro- and nanostructures.

To compare with the available beam-substrate medium models in the literature [11, 48, 57], the simplified strain-gradient nanobeam model on the substrate medium (SSGNS) as proposed by Sae-Long et al. [48] is of interest and was selected for this work. The normalized beam deflections obtained from the proposed model $v_{nor} = v_{\text{Proposed}} / v_{\text{Classical}}$ and from the simplified strain-gradient beam-substrate medium model $v_{nor,s} = v_{\text{SSGNS}} / v_{\text{Classical}}$ with the varied system parameters are shown in Tables 1-4. Based on the SSGNS model, this model is independent of the phase parameter α, resulting in a constant of $v_{nor,s}$ along the variation of α for all cases. The difference between both models increases with the reduction of the mixture parameter α, especially with the lower value of the non-dimensional substrate-stiffness parameter $\bar{K}_{sub}$ but the higher value of the material length scale parameter L_c.

3.4. Example IV: parametric study of system parameters on the beam deflection

This simulation examines the bulk Young's modulus E_{xx} of the local model, which is comparable to the proposed model with the nonlocal and surface effects included. Therefore, these obtained bulk Young's moduli are defined as the "*effective bulk Young's modulus (EBYM)*" E_{bulk}^{eff} [87], which represents and implies the size-scale and size-dependent effects within the micro- and nanostructures [9, 18, 28, 32]. A silver cantilever nanobeam system on the elastic substrate medium subjected to an end load P_{end} = 10 nN, as seen in Fig. 10, is used to investigate the variation of the system parameters on the EBYM in this study. The material properties of the silver nanobeam are given by He and Lilley [87]. The bulk Young's modulus is E_{xx} = 76 GPa, while the surface elastic modulus E_{xx}^{sur} and its residual surface stress τ_{res}^{sur} are 1.22 nN/mm and 0.89 nN/mm, respectively. The geometric properties of the nanobeam follow those used by Limkatanyu et al. [11, 28], such as the nanobeam's length L of 1,000 nm with a 100x100 nm^2 square cross-section as well as simulation III. In order to investigate the variation of the system parameters on the EBYM, this study varies the mixture parameter α with a range of $0 \le \alpha \le 1$, while the material length-scale parameter is normalized with a range of $0 \le \xi_c = L_c / L \le 1$. The non-dimensional substrate-stiffness parameter $\bar{K}_{sub}$ ranges from 1 to 100, as used by Demir et al. [69], and can be computed from Eq. (36).

As proposed by He and Lilley [87], the EBYM E_{bulk}^{eff} can be determined from Eq. (37). First, the end transverse displacement v_{end} of the proposed model is calculated. Then, the obtained displacement is substituted into Eq. (37), while the EBYM E_{bulk}^{eff} is obtained by solving this nonlinear relation. It is worth noting that the right-hand side of Eq. (37) represents the end transverse displacement of the local beam-substrate medium model, while the left-hand side of Eq. (37) is addressed with the transverse displacement, including the nonlocal and surface effects:

$$v_{end} = \frac{\sqrt{2}P_{end}}{E_{bulk}^{eff} I \left(k_{sub} / E_{bulk}^{eff} I\right)^{3/4}} \left[\frac{\sinh\left(\sqrt{2}L\left(k_{sub} / E_{bulk}^{eff} I\right)^{1/4}\right) - \sin\left(\sqrt{2}L\left(k_{sub} / E_{bulk}^{eff} I\right)^{1/4}\right)}{2 + \cos\left(\sqrt{2}L\left(k_{sub} / E_{bulk}^{eff} I\right)^{1/4}\right) + \cosh\left(\sqrt{2}L\left(k_{sub} / E_{bulk}^{eff} I\right)^{1/4}\right)} \right] \tag{37}$$

Figure 11 presents the distribution of the EBYM E_{bulk}^{eff} with the system parameter variations. Based on the system parameters, only the solution of Case I $(\Delta = \eta^3 + \Xi^2 > 0)$ in Appendix A is activated for this case study. This diagram reveals that the EBYM increases with the mixture parameter α, especially in the purely nonlocal phase $(\alpha \to 0)$ with the higher value of the material length scale parameter L_c but the lower value of the non-dimensional substrate-stiffness parameter $\bar{K}_{sub}$ (softer substrate medium), as observed at Point A. In addition to the nonlocal effect, the surface-energy effect leads to an increase in the EBYM when compared to the initial bulk Young's modulus, as seen at Point B. Because the stiffening phenomenon caused by the surface-energy effect is independent of both the mixture parameter α and the nonlocal parameter ξ_c, the EBYM increases with a constant relationship. However, the influence of both nonlocal and surface-energy effects on the EBYM is reduced when the substrate medium is stiffened (an increase in the non-dimensional substrate-stiffness parameter $\bar{K}_{sub}$). This stiffening phenomenon caused by the nonlocal, surface-energy, and substrate-structure interaction effects corresponds to the observations in Simulation II and to those available in the literature [11, 28, 48, 49].

Table 1. Normalized beam deflection obtained from the proposed model υ_{nor} and the simplified strain-gradient beam-substrate medium model $\upsilon_{nor,s}$ with the non-dimensional substrate-stiffness parameter of $\overline{K}_{sub} = 1$.

	$\xi_c = 0$			$\xi_c = 0.05$			$\xi_c = 0.10$			$\xi_c = 0.15$			$\xi_c = 0.20$		
α	υ_{nor}	$\upsilon_{nor,s}$	%Δ	υ_{nor}	$\upsilon_{nor,s}$	%Δ	υ_{nor}	$\upsilon_{nor,s}$	%Δ	υ_{nor}	$\upsilon_{nor,s}$	%Δ	υ_{nor}	$\upsilon_{nor,s}$	%Δ
0	0.7210	0.7210	0.00	0.6799	0.7174	5.51	0.6397	0.7084	10.74	0.6009	0.6960	15.83	0.5644	0.6823	20.89
0.1	0.7210	0.7210	0.00	0.6841	0.7174	4.87	0.6481	0.7084	9.30	0.6136	0.6960	13.43	0.5813	0.6823	17.37
0.2	0.7210	0.7210	0.00	0.6883	0.7174	4.23	0.6565	0.7084	7.90	0.6262	0.6960	11.15	0.5979	0.6823	14.11
0.3	0.7210	0.7210	0.00	0.6924	0.7174	3.61	0.6648	0.7084	6.55	0.6386	0.6960	8.99	0.6143	0.6823	11.08
0.4	0.7210	0.7210	0.00	0.6966	0.7174	2.99	0.6731	0.7084	5.25	0.6508	0.6960	6.94	0.6303	0.6823	8.26
0.5	0.7210	0.7210	0.00	0.7007	0.7174	2.39	0.6812	0.7084	3.99	0.6629	0.6960	5.00	0.6461	0.6823	5.62
0.6	0.7210	0.7210	0.00	0.7048	0.7174	1.79	0.6893	0.7084	2.77	0.6748	0.6960	3.14	0.6615	0.6823	3.14
0.7	0.7210	0.7210	0.00	0.7088	0.7174	1.21	0.6973	0.7084	1.58	0.6866	0.6960	1.38	0.6768	0.6823	0.82
0.8	0.7210	0.7210	0.00	0.7129	0.7174	0.63	0.7053	0.7084	0.44	0.6982	0.6960	0.31	0.6917	0.6823	1.36
0.9	0.7210	0.7210	0.00	0.7169	0.7174	0.07	0.7131	0.7084	0.67	0.7096	0.6960	1.92	0.7065	0.6823	3.42
1	0.7210	0.7210	0.00	0.7210	0.7174	0.49	0.7210	0.7084	1.75	0.7210	0.6960	3.46	0.7210	0.6823	5.36

Note: ξ_c denotes normalized material length scale parameter; α denotes mixture parameter; %Δ denotes percentage difference; υ_{nor} and $\upsilon_{nor,s}$ denote the normalized beam deflections of the proposed model and SSGNS model, respectively.

Table 2. Normalized beam deflection obtained from the proposed model υ_{nor} and the simplified strain-gradient beam-substrate medium model $\upsilon_{nor,s}$ with the non-dimensional substrate-stiffness parameter of $\overline{K}_{sub} = 4$.

	$\xi_c = 0$			$\xi_c = 0.05$			$\xi_c = 0.10$			$\xi_c = 0.15$			$\xi_c = 0.20$		
α	υ_{nor}	$\upsilon_{nor,s}$	%Δ	υ_{nor}	$\upsilon_{nor,s}$	%Δ	υ_{nor}	$\upsilon_{nor,s}$	%Δ	υ_{nor}	$\upsilon_{nor,s}$	%Δ	υ_{nor}	$\upsilon_{nor,s}$	%Δ
0	0.7573	0.7573	0.00	0.7219	0.7543	4.49	0.6859	0.7468	8.88	0.6502	0.7366	13.29	0.6158	0.7252	17.78
0.1	0.7573	0.7573	0.00	0.7255	0.7543	3.96	0.6935	0.7468	7.69	0.6619	0.7366	11.29	0.6316	0.7252	14.83
0.2	0.7573	0.7573	0.00	0.7292	0.7543	3.45	0.7010	0.7468	6.54	0.6734	0.7366	9.40	0.6470	0.7252	12.09
0.3	0.7573	0.7573	0.00	0.7328	0.7543	2.94	0.7083	0.7468	5.44	0.6846	0.7366	7.61	0.6620	0.7252	9.55
0.4	0.7573	0.7573	0.00	0.7363	0.7543	2.44	0.7156	0.7468	4.36	0.6956	0.7366	5.91	0.6767	0.7252	7.18
0.5	0.7573	0.7573	0.00	0.7399	0.7543	1.95	0.7228	0.7468	3.33	0.7063	0.7366	4.29	0.6909	0.7252	4.97
0.6	0.7573	0.7573	0.00	0.7434	0.7543	1.47	0.7299	0.7468	2.33	0.7169	0.7366	2.75	0.7049	0.7252	2.89
0.7	0.7573	0.7573	0.00	0.7469	0.7543	0.99	0.7368	0.7468	1.36	0.7273	0.7366	1.29	0.7184	0.7252	0.95
0.8	0.7573	0.7573	0.00	0.7504	0.7543	0.52	0.7437	0.7468	0.42	0.7375	0.7366	0.11	0.7317	0.7252	0.88
0.9	0.7573	0.7573	0.00	0.7538	0.7543	0.06	0.7505	0.7468	0.49	0.7475	0.7366	1.45	0.7446	0.7252	2.60
1	0.7573	0.7573	0.00	0.7573	0.7543	0.39	0.7573	0.7468	1.38	0.7573	0.7366	2.72	0.7573	0.7252	4.23

Note: ξ_c denotes normalized material length scale parameter; α denotes mixture parameter; %Δ denotes percentage difference; υ_{nor} and $\upsilon_{nor,s}$ denote the normalized beam deflections of the proposed model and SSGNS model, respectively.

Table 3. Normalized beam deflection obtained from the proposed model υ_{nor} and the simplified strain-gradient beam-substrate medium model $\upsilon_{nor,s}$ with the non-dimensional substrate-stiffness parameter of $\overline{K}_{sub} = 7$.

	$\xi_c = 0$			$\xi_c = 0.05$			$\xi_c = 0.10$			$\xi_c = 0.15$			$\xi_c = 0.20$		
α	υ_{nor}	$\upsilon_{nor,s}$	%Δ	υ_{nor}	$\upsilon_{nor,s}$	%Δ	υ_{nor}	$\upsilon_{nor,s}$	%Δ	υ_{nor}	$\upsilon_{nor,s}$	%Δ	υ_{nor}	$\upsilon_{nor,s}$	%Δ
0	0.7845	0.7845	0.00	0.7538	0.7820	3.73	0.7217	0.7757	7.49	0.6889	0.7672	11.36	0.6566	0.7577	15.40
0.1	0.7845	0.7845	0.00	0.7570	0.7820	3.29	0.7284	0.7757	6.49	0.6996	0.7672	9.67	0.6713	0.7577	12.88
0.2	0.7845	0.7845	0.00	0.7602	0.7820	2.87	0.7351	0.7757	5.52	0.7099	0.7672	8.07	0.6855	0.7577	10.54
0.3	0.7845	0.7845	0.00	0.7633	0.7820	2.44	0.7416	0.7757	4.60	0.7201	0.7672	6.55	0.6992	0.7577	8.37
0.4	0.7845	0.7845	0.00	0.7664	0.7820	2.03	0.7481	0.7757	3.70	0.7299	0.7672	5.11	0.7125	0.7577	6.34
0.5	0.7845	0.7845	0.00	0.7695	0.7820	1.62	0.7544	0.7757	2.83	0.7396	0.7672	3.74	0.7254	0.7577	4.45
0.6	0.7845	0.7845	0.00	0.7725	0.7820	1.22	0.7606	0.7757	1.99	0.7490	0.7672	2.44	0.7380	0.7577	2.68
0.7	0.7845	0.7845	0.00	0.7755	0.7820	0.83	0.7667	0.7757	1.17	0.7581	0.7672	1.20	0.7501	0.7577	1.01
0.8	0.7845	0.7845	0.00	0.7785	0.7820	0.44	0.7727	0.7757	0.39	0.7671	0.7672	0.01	0.7619	0.7577	0.55
0.9	0.7845	0.7845	0.00	0.7815	0.7820	0.06	0.7786	0.7757	0.38	0.7759	0.7672	1.12	0.7733	0.7577	2.02
1	0.7845	0.7845	0.00	0.7845	0.7820	0.32	0.7845	0.7757	1.12	0.7845	0.7672	2.20	0.7845	0.7577	3.41

Note: ξ_c denotes normalized material length scale parameter; α denotes mixture parameter; %Δ denotes percentage difference; υ_{nor} and $\upsilon_{nor,s}$ denote the normalized beam deflections of the proposed model and SSGNS model, respectively.

Table 4. Normalized beam deflection obtained from the proposed model υ_{nor} and the simplified strain-gradient beam-substrate medium model $\upsilon_{nor,s}$ with the non-dimensional substrate-stiffness parameter of $\bar{K}_{sub}=10$.

	$\xi_c=0$			$\xi_c=0.05$			$\xi_c=0.10$			$\xi_c=0.15$			$\xi_c=0.20$		
α	υ_{nor}	$\upsilon_{nor,s}$	%Δ	υ_{nor}	$\upsilon_{nor,s}$	%Δ	υ_{nor}	$\upsilon_{nor,s}$	%Δ	υ_{nor}	$\upsilon_{nor,s}$	%Δ	υ_{nor}	$\upsilon_{nor,s}$	%Δ
0	0.8056	0.8056	0.00	0.7789	0.8034	3.15	0.7500	0.7981	6.41	0.7200	0.7910	9.86	0.6897	0.7830	13.53
0.1	0.8056	0.8056	0.00	0.7817	0.8034	2.78	0.7561	0.7981	5.56	0.7296	0.7910	8.40	0.7033	0.7830	11.34
0.2	0.8056	0.8056	0.00	0.7844	0.8034	2.42	0.7620	0.7981	4.73	0.7390	0.7910	7.03	0.7163	0.7830	9.31
0.3	0.8056	0.8056	0.00	0.7872	0.8034	2.06	0.7678	0.7981	3.94	0.7482	0.7910	5.72	0.7289	0.7830	7.42
0.4	0.8056	0.8056	0.00	0.7899	0.8034	1.71	0.7735	0.7981	3.18	0.7570	0.7910	4.48	0.7410	0.7830	5.67
0.5	0.8056	0.8056	0.00	0.7925	0.8034	1.37	0.7791	0.7981	2.43	0.7657	0.7910	3.30	0.7527	0.7830	4.03
0.6	0.8056	0.8056	0.00	0.7952	0.8034	1.03	0.7846	0.7981	1.72	0.7741	0.7910	2.18	0.7640	0.7830	2.49
0.7	0.8056	0.8056	0.00	0.7978	0.8034	0.70	0.7900	0.7981	1.02	0.7823	0.7910	1.11	0.7749	0.7830	1.04
0.8	0.8056	0.8056	0.00	0.8004	0.8034	0.37	0.7953	0.7981	0.35	0.7902	0.7910	0.09	0.7855	0.7830	0.31
0.9	0.8056	0.8056	0.00	0.8030	0.8034	0.05	0.8005	0.7981	0.30	0.7980	0.7910	0.88	0.7957	0.7830	1.59
1	0.8056	0.8056	0.00	0.8056	0.8034	0.27	0.8056	0.7981	0.93	0.8056	0.7910	1.81	0.8056	0.7830	2.80

Note: ξ_c denotes normalized material length scale parameter; α denotes mixture parameter; %Δ denotes percentage difference; υ_{nor} and $\upsilon_{nor,s}$ denote the normalized beam deflections of the proposed model and SSGNS model, respectively.

4. Conclusions

The present work introduces a new beam-substrate medium model for analyzing the bending of a nanobeam system on a substrate medium. The proposed model incorporates the coupling interaction among nonlocality, surface energy, and substrate-structure interaction. The stress-induced mixture of integral elasticity is utilized to tackle the intrinsic nonlocality of micro- and nano-sized beams. The Gurtin-Murdoch continuum surface model characterizes the surface-energy effect, while the interaction between the nanobeam and the underlying substrate medium is modeled using the Winkler-based foundation model. The governing differential equation (GDE) and associated boundary conditions of the proposed model are developed using the virtual displacement principle. Four numerical simulations are employed to analyze the behaviors and properties of nanobeam systems, and the findings are as follows:

- The softening phenomenon is observed when the mixture parameter decreases. Conversely, if the mixture parameter increases, the system stiffness will increase. Thus, nonlocality leads to the stiffening of system stiffness due to the enhancement of system rigidity by increasing the material length-scale parameter and reducing the mixture parameter.
- The response of the simplified strain-gradient beam model [48] corresponds to one of the scenarios obtained from the proposed mixture two-phase nonlocal beam model.
- Both surface energy and substrate-structure interaction result in the enhancement of system stiffness and are important factors in the bending analysis of nanobeam systems on the elastic substrate medium.
- The surface energy effect enhances system stiffness, but this effect diminishes as the substrate medium becomes stiffer.
- The increase in system stiffness caused by nonlocality and surface energy leads to a reduction in normalized beam deflection but an increase in effective bulk Young's modulus (EBYM), particularly in a softer substrate medium.

The future direction of this project involves enhancing the proposed nonlocal beam-substrate model by incorporating both material and geometric nonlinearities. Consequently, this would yield a more reasonable representation of the nanostructure and prove advantageous for future research in the fields of nanoscience and nanoengineering.

Author Contributions

S. Limkatanyu played a role in validation, formal analysis, investigation, writing and revising the manuscript and supervision; W. Sae-Long played a role in conceptualization, methodology, software, validation, formal analysis, investigation, data curation, writing and revising the manuscript, visualization, supervision, project administration, funding acquisition; J. Rungamornrat played a role in investigation and data curation; N. Damrongwiriyanupap played a role in investigation; S. Keawsawasvong played a role in investigation; P. Sukontasukkul played roles in investigation and supervision; C. Hansapinyo played roles in investigation. The manuscript was written through the contribution of all authors. All authors discussed the results, reviewed, and approved the final version of the manuscript.

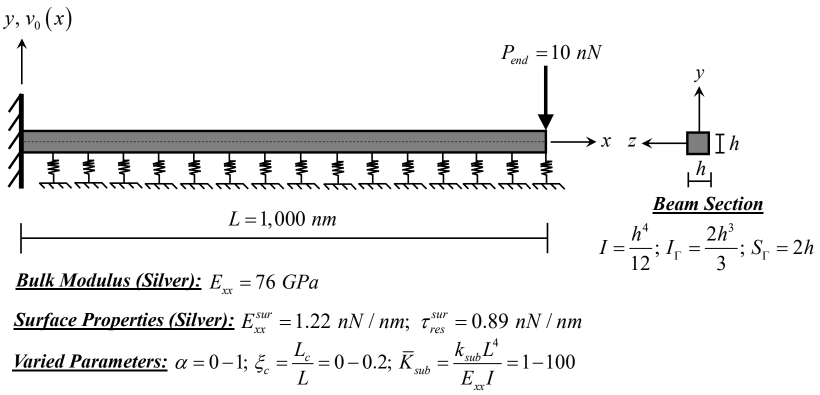

Fig. 10. Simulation IV: parametric study of system parameters on the EBYM.

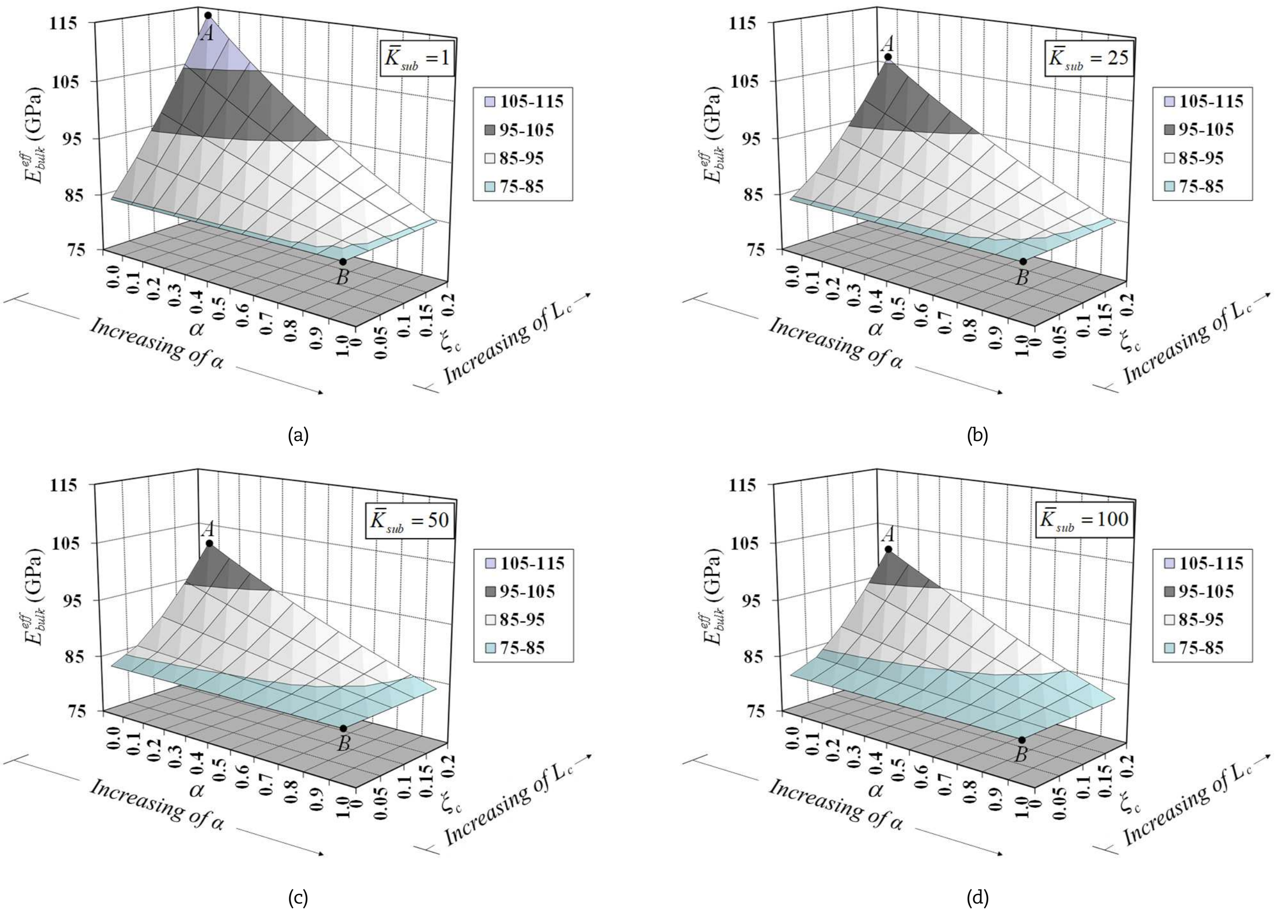

Fig. 11. Variation of EBYM E_{bulk}^{eff} with variation on mixture parameter α, normalized material length scale parameter ξ_c and non-dimensional substrate-stiffness parameter: (a) $\bar{K}_{sub} = 1$; (b) $\bar{K}_{sub} = 25$; (c) $\bar{K}_{sub} = 50$; and (d) $\bar{K}_{sub} = 100$.

Acknowledgments

This study was financially supported by University of Phayao and Thailand Science Research and Innovation Fund (Fundamental Fund 2024).

Conflict of Interest

The authors declared no potential conflicts of interest concerning the research, authorship, and publication of this article.

Funding

This study was financially supported by University of Phayao and Thailand Science Research and Innovation Fund (Fundamental Fund 2024).

Data Availability Statements

The datasets generated and/or analyzed during the current study are available from the corresponding author on reasonable request.

References

[1] Bachiri, A., Daikh, A.A., Tounsi, A., On the thermo-elastic response of FG-CNTRC cross-ply laminated plates under temperature loading using a new HSDT, *Journal of Applied and Computational Mechanics*, 8(4), 2022, 1370-1386.
[2] Botkin, N.D., Turova, V.L., Mathematical models of a biosensor, *Applied Mathematical Modelling*, 28, 2004, 573-589.
[3] Guo, C., Xu, L., Su, Y., Li, H., Zhang, M., Yang, Y., Stretchable nanogenerators for scavenging mechanical energy, *Nano Research*, 16, 2023, 11682-11697.
[4] Cao, Z., Wang, K.F., Wang, B.L., Nonlinear analysis of flexoelectric acoustic energy harvesters with Helmholtz resonator, *Applied Mathematical Modelling*, 129, 2024, 633-654.
[5] Agahi, M., Rahaie, M., A novel DNA tweezers-based nanobiosensor for multiple detections of circulating exosomal microRNAs in breast cancer, *Analytical Biochemistry*, 651, 2022, 114697.
[6] Eltaher, M.A., Khater, M.E., Park, S., Abdel-Rahman, E., Yavuz, M., On the static stability of nonlocal nanobeams using higher-order beam theories, *Advances in Nano Research*, 4(1), 2016, 51-64.
[7] Pinnola, F.P., Ali Faghidian, S., Barretta, R., Marotti de Sciarra, F., Variationally consistent dynamics of nonlocal gradient elastic beams, *International Journal of Engineering Science*, 149, 2020, 103220.
[8] Oskouie, M.F., Rouhi, H., Hybrid strain- and stress-driven integral non-local model, *The European Physical Journal Plus*, 136, 2021, 823.

[9] Sae-Long, W., Limkatanyu, S., Sukontasukkul, P., Damrongwiriyanupap, N., Rungamornrat, J., Prachasaree, W., Fourth-order strain gradient bar-substrate model with nonlocal and surface effects for the analysis of nanowires embedded in substrate media, *Facta Universitatis, Series: Mechanical Engineering*, 19(4), 2021, 657-680.
[10] Darban, H., Luciano, R., Basista, M., Calibration of the length scale parameter for the stress-driven nonlocal elasticity model from quasi-static and dynamic experiments, *Mechanics of Advanced Materials and Structures*, 30(17), 2023, 3518-3524.
[11] Limkatanyu, S., Sae-Long, W., Rungamornrat, J., Buachart, C., Sukontasukkul, P., Keawsawasvong, S., Chindaprasirt, P., Bending, buckling and free vibration analyses of nanobeam-substrate medium systems, *Facta Universitatis, Series: Mechanical Engineering,* 20(3), 2022, 561-587.
[12] Mensah, K., Abdelmageed, A.M., Shokry, H., Effect of eggshell/N,N-dimethylformamide (DMF) mixing ratios on the sonochemical production of $CaCO_3$ nanoparticles, *Journal of Engineering and Applied Science*, 69, 2022, 16.
[13] Lam, D.C.C., Yang, F., Chong, A.C.M., Wang, J., Tong, P., Experiments and theory in strain gradient elasticity, *Journal of the Mechanics and Physics of Solids*, 51(8), 2003, 1477-1508.
[14] Gupta, A.K., Nair, P.R., Akin, D., Ladisch, M.R., Broyles, S., Alam, M.A., Bashir, R., Anomalous resonance in a nanomechanical biosensor, *Applied Physical Sciences*, 103(36), 2006, 13362-13367.
[15] Tang, C., Alici, G., Evaluation of length-scale effects for mechanical behaviour of micro- and nanocantilevers: II. Experimental verification of deflection models using atomic force microscopy, *Journal of Physics D: Applied Physics*, 44(33), 2011, 335502.
[16] Harris, K.D., Elias, A.L., Chung, H.J., Flexible electronics under strain: a review of mechanical characterization and durability enhancement strategies, *Journal of Materials Science*, 51, 2016, 2771-2805.
[17] Xu, D., Wang, Z., Chen, L., Thaiyanurak, T., Atomic mechanisms of crystallization in nano-sized metallic glasses, *Crystals*, 13(1), 2023, 32.
[18] Limkatanyu, S., Damrongwiriyanupap, N., Prachasaree, W., Sae-Long, W., Modeling of axially loaded nanowires embedded in elastic substrate media with inclusion of nonlocal and surface effects, *Journal of Nanomaterials*, 2013, 2013, 635428.
[19] Sae-Long, W., Limkatanyu, S., Prachasaree, W., Rungamornrat, J., Sukontasukkul, P., A thermodynamics-based nonlocal bar-elastic substrate model with inclusion of surface-energy effect, *Journal of Nanomaterials*, 2020, 2020, 8276745.
[20] Barretta, R., Canadija, M., Marotti de Sciarra, F., Skoblar, A., Free vibrations of Bernoulli-Euler nanobeams with point mass interacting with heavy fluid using nonlocal elasticity, *Nanomaterials*, 12(15), 2022, 2676.
[21] Wagner, G.J., Liu, W.K., Coupling of atomistic and continuum simulations using a bridging scale decomposition, *Journal of Computational Physics*, 190(1), 2003, 249-274.
[22] Poluektov, M., Eriksson, O., Kreiss, G., Coupling atomistic and continuum modelling of magnetism, *Computer Methods in Applied Mechanics and Engineering*, 329, 2018, 219-253.
[23] Liew, K.M., He, X.Q., Kitipornchai, S., Buckling characteristics of embedded multi-walled carbon nanotubes, *Proceedings of the Royal Society A*, 461(2064), 2005, 3785-3805.
[24] Narendar, S., Roy Mahapatra, D., Gopalakrishnan, S., Prediction of nonlocal scaling parameter for armchair and zigzag single-walled carbon nanotubes based on molecular structural mechanics, nonlocal elasticity and wave propagation, *International Journal of Engineering Science*, 49(6), 2011, 509-522.
[25] Yang, S., Kim, W., Cho, M., Molecular dynamics study on the coalescence kinetics and mechanical behavior of nanoporous structure formed by thermal sintering of Cu nanoparticles, *International Journal of Engineering Science*, 123, 2018, 1-19.
[26] Umeno, Y., Kubo, A., Wang, C., Shima, H., Diameter-change-induced transition in buckling modes of defective zigzag carbon nanotubes, *Nanomaterials*, 12(15), 2022, 2617.
[27] Intarit, P., Senjuntichai, T., Rungamornrat, J., Rajapakse, R.K.N.D., Penny-shaped crack in elastic medium with surface energy effects, *Acta Mechanica*, 228, 2017, 617-630.
[28] Limkatanyu, S., Sae-Long, W., Horpibulsuk, S., Prachasaree, W., Damrongwiriyanupap, N., Flexural responses of nanobeams with coupled effects of nonlocality and surface energy, *ZAMM – Journal of Applied Mathematics and Mechanics*, 98(10), 2018, 1771-1793.
[29] Barretta, R., Faghidian, S.A., Marotti de Sciarra, F., A consistent variational formulation of Bishop nonlocal rods, *Continuum Mechanics and Thermodynamics*, 32, 2020, 1311-1323.
[30] Naghinejad, M., Ovesy, H.R., Free vibration characteristics of nonlocal viscoelastic nano-scaled plates with rectangular cutout and surface effects, *ZAMM – Journal of Applied Mathematics and Mechanics*, 101(5), 2021, e201900294.
[31] Abouelregal, A.E., Alanazi, R., Sedighi, H.M., Thermal plane waves in unbounded non-local medium exposed to a moving heat source with a non-singular kernel and higher order time derivatives, *Engineering Analysis with Boundary Elements*, 140, 2022, 464-475.
[32] Limkatanyu, S., Sae-Long, W., Mohammad-Sedighi, H., Rungamornrat, J., Sukontasukkul, P., Imjai, T., Zhang, H., Static and free vibration analyses of single-walled carbon nanotube (SWCNT)-substrate medium systems, *Nanomaterials*, 12(10), 2022, 1740.
[33] Faghidian, S.A., Zur, K.K., Rabczuk, T., Mixture unified gradient theory: a consistent approach for mechanics of nanobars, *Applied Physics A*, 128, 2022, 996.
[34] Zhou, Y.T., Tian, X.J., Ding, S.H., Microstructure size-dependent contact behavior of a thermoelectric film bonded to an elastic substrate with couple stress theory, *International Journal of Solids and Structures*, 256, 2022, 111982.
[35] Faghidian, S.A., Mohammad-Sedighi, H., Dynamics of nonlocal thick nano-bars, *Engineering with Computers*, 38, 2022, 2487-2496.
[36] Eringen, A.C., Nonlocal polar elastic continua, *International Journal of Engineering Science*, 10(1), 1972, 1-16.
[37] Eringen, A.C., On differential equations of nonlocal elasticity and solutions of screw dislocation and surface waves, *Journal of Applied Physics*, 54(9), 1983, 4703-4710.
[38] Aranda-Ruiz, J., Loya, J., Fernández-Sáez, J., Bending vibrations of rotating nonuniform nanocantilevers using the Eringen nonlocal elasticity theory, *Composite Structures*, 94(9), 2012, 2990-3001.
[39] Ghafarian, M., Ariaei, A., Free vibration analysis of a multiple rotating nano-beams system based on the Eringen nonlocal elasticity theory, *Journal of Applied Physics*, 120(5), 2016, 054301.
[40] Lignola, G.P., Spena, F.R., Prota, A., Manfredi, G., Exact stiffness–matrix of two nodes Timoshenko beam on elastic medium. An analogy with Eringen model of nonlocal Euler–Bernoulli nanobeams, *Computers & Structures*, 182, 2017, 556-572.
[41] Zhang, Y.P., Challamel, N., Wang, C.M., Zhang, H., Comparison of nano-plate bending behaviour by Eringen nonlocal plate, Hencky bar-net and continualised nonlocal plate models, *Acta Mechanica*, 230, 2019, 885-907.
[42] Mahmoudpour, E., Differences between stress-driven nonlocal integral model and Eringen differential model in the vibrations analysis of carbon nanotubes conveying magnetic nanoflow, *Journal of the Brazilian Society of Mechanical Sciences and Engineering*, 43, 2021, 555.
[43] Kröner, E., Elasticity theory of materials with long range cohesive forces, *International Journal of Solids and Structures*, 3(5), 1967, 731-742.
[44] Krumhansl, J.A., *Some considerations of the relation between solid state physics and generalized continuum mechanics*, In: Kröner, E. (eds) Mechanics of generalized continua, IUTAM Symposia, Springer, Berlin, Heidelberg, 1968.
[45] Kunin, I.A., *The theory of elastic media with microstructure and the theory of dislocations*, In: Kröner, E. (eds) Mechanics of generalized continua, IUTAM Symposia, Springer, Berlin, Heidelberg, 1968.
[46] Peddieson, J., Buchanan, G.B., McNitt, R.P., Application of nonlocal continuum models to nanotechnology, *International Journal of Engineering Science*, 41(3-5), 2003, 305-312.
[47] Shaat, M., Correction of local elasticity for nonlocal residuals: application to Euler–Bernoulli beams, *Meccanica*, 53, 2018, 3015-3035.
[48] Sae-Long, W., Limkatanyu, S., Rungamornrat, J., Prachasaree, W., Sukontasukkul, P., Sedighi, H.M., A rational beam-elastic substrate model with incorporation of beam-bulk nonlocality and surface-free energy, *The European Physical Journal Plus*, 136, 2021, 80.
[49] Limkatanyu, S., Sae-Long, W., Sedighi, H.M., Rungamornrat, J., Sukontasukkul, P., Zhang, H., Chindaprasirt, P., Flexibility-based stress-driven nonlocal frame element: formulation and applications, *Engineering with Computers*, 39, 2023, 399-417.
[50] Romano, G., Barretta, R., Diaco, M., Marotti de Sciarra, F., Constitutive boundary conditions and paradoxes in nonlocal elastic nanobeams, *International Journal of Mechanical Sciences*, 121, 2017, 151-156.
[51] Fernández-Sáez, J., Zaera, R., Loya, J.A., Reddy, J.N., Bending of Euler–Bernoulli beams using Eringen's integral formulation: A paradox resolved, *International Journal of Engineering Science*, 99, 2016, 107-116.
[52] Zhu, X., Wang, Y., Dai, H.-H., Buckling analysis of Euler–Bernoulli beams using Eringen's two-phase nonlocal model, *International Journal of Engineering Science*, 116, 2017, 130-140.

[53] Barretta, R., Ali Faghidian, S., Luciano, R., Medaglia, C.M., Penna, R., Stress-driven two-phase integral elasticity for torsion of nano-beams, *Composites Part B: Engineering*, 145, 2018, 62-69.
[54] Vaccaro, M.S., Pinnola, F.P., Marotti de Sciarra, F., Barretta, R., Dynamics of stress-driven two-phase elastic beams, *Nanomaterials*, 11(5), 2021, 1138.
[55] Vaccaro, M.S., Pinnola, F.P., Marotti de Sciarra, F., Canadija, M., Barretta, R., Stress-driven two-phase integral elasticity for Timoshenko curved beams, *Proceedings of the Institution of Mechanical Engineers, Part N: Journal of Nanomaterials, Nanoengineering and Nanosystems*, 235(1-2), 2021, 52-63.
[56] Behdad, S., Arefi, M., A mixed two-phase stress/strain driven elasticity: In applications on static bending, vibration analysis and wave propagation, *European Journal of Mechanics - A/Solids*, 94, 2022, 104558.
[57] Sae-Long, W., Limkatanyu, S., Damrongwiriyanupap, N., Imjai, T., Sukontasukkul, P., Kwon, M., Hansapinyo, C., Finite beam element based on the strain-driven model for analyses of nanobeams on substrate media, *Suranaree Journal of Science & Technology*, 29(5), 2022, 010162.
[58] Romano, G., Barretta, R., Diaco, M., On nonlocal integral models for elastic nano-beams, *International Journal of Mechanical Sciences*, 131-132, 2017, 490-499.
[59] Luciano, R., Caporale, A., Darban, H., Bartolomeo, C., Variational approaches for bending and buckling of non-local stress-driven Timoshenko nano-beams for smart materials, *Mechanics Research Communications*, 103, 2020, 103470.
[60] Vaccaro, M.S., Sedighi, H.M., Two-phase elastic axisymmetric nanoplates, *Engineering with Computers*, 39, 2023, 827-834.
[61] Gurtin, M.E., Murdoch, A.I., A continuum theory of elastic material surfaces, *Archive for Rational Mechanics and Analysis*, 57, 1975, 291-323.
[62] Gurtin, M.E., Murdoch, A.I., Surface stress in solids, *International Journal of Solids and Structures*, 14(6), 1978, 431-440.
[63] Cammarata, R.C., Surface and interface stress effects in thin films, *Progress in Surface Science*, 46(1), 1994, 1-38.
[64] Juntarasaid, C., Pulngern, T., Chucheepsakul, S., Bending and buckling of nanowires including the effects of surface stress and nonlocal elasticity, *Physica E: Low-dimensional Systems and Nanostructures*, 46, 2012, 68-76.
[65] Nazarenko, L., Bargmann, S., Stolarski, H., Closed-form formulas for the effective properties of random particulate nanocomposites with complete Gurtin–Murdoch model of material surfaces, *Continuum Mechanics and Thermodynamics*, 29, 2017, 77-96.
[66] Baranova, S., Mogilevskaya, S.G., Mantic, V., Jiménez-Alfaro, S., Analysis of the antiplane problem with an embedded zero thickness layer described by the Gurtin-Murdoch model, *Journal of Elasticity*, 140, 2020, 171-195.
[67] Lu, P., Liu, R., Zhai, H., Wang, G., Yu, P., Lu, C., A modified beam model based on Gurtin–Murdoch surface elasticity theory, *Meccanica*, 56, 2021, 1147-1164.
[68] Mogilevskaya, S.G., Zemlyanova, A.Y., Mantic, V., The use of the Gurtin-Murdoch theory for modeling mechanical processes in composites with two-dimensional reinforcements, *Composites Science and Technology*, 210, 2021, 108751.
[69] Demir, C., Mercan, K., Numanoglu, H.M., Civalek, O., Bending response of nanobeams resting on elastic foundation, *Journal of Applied and Computational Mechanics*, 4(2), 2018, 105-114.
[70] Togun, N., Bagdatli, S.M., The vibration of nanobeam resting on elastic foundation using modified couple stress theory, *Tehnicki Glasnik*, 12(4), 2018, 221-225.
[71] Luo, T., Mao, Q., Zeng, S., Wang, K., Wang, B., Wu, J., Lu, Z., Scale effect on the nonlinear vibration of piezoelectric sandwich nanobeams on Winkler foundation, *Journal of Vibration Engineering & Technologies*, 9, 2021, 1289-1303.
[72] Karmakar, S., Chakraverty, S., Thermal vibration of nonhomogeneous Euler nanobeam resting on Winkler foundation, *Engineering Analysis with Boundary Elements*, 140, 2022, 581-591.
[73] Zheng, Y.-F., Qu, D.-Y., Liu, L.-C., Chen, C.-P., Size-dependent nonlinear bending analysis of nonlocal magneto-electro-elastic laminated nanobeams resting on elastic foundation, *International Journal of Non-Linear Mechanics*, 148, 2023, 104255.
[74] Winkler, E., *Die Lehre von der und Festigkeit*, Dominicus, Prague, Czechoslovakia, 1867.
[75] Ghazwani, M.H., Alnujaie, A., Vinh, P.V., Civalek, Ö., High frequency analysis of the functionally graded sandwich nanobeams embedded in elastic foundations using nonlocal quasi-3D theory, *Physica B: Condensed Matter*, 675, 2024, 415646.
[76] Ghazwani, M.H., Alnujaie, A., Tounsi, A., Vinh, P.V., On the high-frequency analysis of exponentially graded nanobeams resting on Winkler–Pasternak foundations, *Journal of Vibration Engineering & Technologies*, 2024, https://doi.org/10.1007/s42417-024-01348-6.
[77] Wolfram, S., *Mathematica reference guide*, Addison-Wesley Publishing Company, Redwood City, California, USA, 1992.
[78] Öchsner, A., *Classical beam theories of structural mechanics*, Springer Cham, Switzerland, 2021.
[79] Miller, R.E., Shenoy, V.B., Size-dependent elastic properties of nanosized structural elements, *Nanotechnology*, 11(3), 2000, 139-147.
[80] Barretta, R., Fabbrocino, F., Luciano, R., Marotti de Sciarra, F., Closed-form solutions in stress-driven two-phase integral elasticity for bending of functionally graded nano-beams, *Physica E: Low-dimensional Systems and Nanostructures*, 97, 2018, 13-30.
[81] Limkatanyu, S., Sae-Long, W., Prachasaree, W., Kwon, M., Improved nonlinear displacement-based beam element on a two-parameter foundation, *European Journal of Environmental and Civil Engineering*, 19(6), 2015, 649-671.
[82] Morfidis, K., *Research and development of methods for the modeling of foundation structural elements and soil*, PhD Dissertation, Department of Civil Engineering, Aristotle University of Thessaloniki, 2003.
[83] Avramidis, I.E., Morfidis, K., Bending of beams on three-parameter elastic foundation, *International Journal of Solids and Structures*, 43(2), 2006, 357-375.
[84] Romano, G., Barretta, R., Nonlocal elasticity in nanobeams: the stress-driven integral model, *International Journal of Engineering Science*, 115, 2017, 14-27.
[85] Cuenot, S., Frétigny, C., Champagne, S.D., Nysten, B., Surface tension effect on the mechanical properties of nanomaterials measured by atomic force microscopy, *Physical Review B*, 69, 2004, 165410.
[86] Wan, J., Fan, Y.L., Gong, D.W., Shen, S.G., Fan, X.Q., Surface relaxation and stress of fcc metals: Cu, Ag, Au, Ni, Pd, Pt, Al and Pb, *Modelling and Simulation in Materials Science and Engineering*, 7(2), 1999, 189-206.
[87] He, J., Lilley, C.M., Surface effect on the elastic behavior of static bending nanowires, *Nano Letters*, 8(7), 2008, 1798-1802.

Appendix A

The general form of the differential equation of Eqs. (31) can be expressed as:

$$\frac{d^6\upsilon(x)}{dx^6}+\lambda_1\frac{d^4\upsilon(x)}{dx^4}+\lambda_2\frac{d^2\upsilon(x)}{dx^2}+\lambda_3\upsilon(x)=0 \tag{A.1}$$

Parameters λ_1, λ_2, and λ_3 in Eq. (A.1) can be defined as:

$$\lambda_1=-\frac{(EI)_{eff}^{L}}{(EI)_{eff}^{H}};\ \lambda_2=\frac{(K)_{eff}^{H}}{(EI)_{eff}^{H}};\ \text{and}\ \lambda_3=-\frac{k_{sub}}{(EI)_{eff}^{H}} \tag{A.2}$$

For the sake of conciseness, the parameters λ_1, λ_2, and λ_3 in Eq. (A.2) are rewritten in terms of the auxiliary parameters for the expression of the general solution as:

$$\eta=\frac{-(\lambda_1^2/3)+\lambda_2}{3};\ \Xi=\frac{(2\lambda_1^3/27)-(\lambda_1\lambda_2/3)+\lambda_3}{2};\ \text{and}\ \Delta=\eta^3+\Xi^2 \tag{A.3}$$

The general form of homogeneous solution of Eq. (A.1) can be expressed as:

$$v_h(x) = \gamma_1(x)C_1 + \gamma_2(x)C_2 + \gamma_3(x)C_3 + \gamma_4(x)C_4 + \gamma_5(x)C_5 + \gamma_6(x)C_6 \tag{A.4}$$

As suggested by Morfidis [80] and Avramidis and Morfidis [81], there are two possible homogeneous solutions, which depend on the sign of the parameter Δ as follows:

Solution Case I: when $\Delta = \eta^3 + \Xi^2 > 0$

$$\begin{aligned} &\gamma_1(x) = e^{R_1 x}; \quad \gamma_2(x) = e^{-R_1 x}; \quad \gamma_3(x) = e^{Rx}\cos[Qx]; \\ &\gamma_4(x) = e^{Rx}\sin[Qx]; \quad \gamma_5(x) = e^{-Rx}\cos[Qx]; \quad \gamma_6(x) = e^{-Rx}\sin[Qx] \end{aligned} \tag{A.5}$$

where

$$\begin{aligned} &R_1 = \sqrt{\sqrt[3]{-\Xi + \sqrt{\Delta}} + \sqrt[3]{-\Xi - \sqrt{\Delta}} - \frac{\lambda_1}{3}}; \; R = \sqrt{\frac{\left(\sqrt{m^2 + n^2} + m\right)}{2}}; \; Q = \sqrt{\frac{\left(\sqrt{m^2 + n^2} - m\right)}{2}} \\ &m = -\frac{\left[\sqrt[3]{-\Xi + \sqrt{\Delta}} + \sqrt[3]{-\Xi - \sqrt{\Delta}} + (2\lambda_1 / 3)\right]}{2}; \; n = \frac{\sqrt{3}\left[\sqrt[3]{-\Xi + \sqrt{\Delta}} - \sqrt[3]{-\Xi - \sqrt{\Delta}}\right]}{2} \end{aligned} \tag{A.6}$$

Solution Case II: when $\Delta = \eta^3 + \Xi^2 < 0$

$$\gamma_1(x) = e^{Rx}; \; \gamma_2(x) = e^{-Rx}; \; \gamma_3(x) = e^{R_1 x}; \; \gamma_4(x) = e^{R_2 x}; \; \gamma_5(x) = e^{-R_1 x}; \; \gamma_6(x) = e^{-R_2 x} \tag{A.7}$$

where

$$\begin{aligned} &R = \sqrt{2\sqrt{-\eta}\cos\left[\frac{\varphi}{3}\right] - \frac{\lambda_1}{3}}; \; R_1 = \sqrt{2\sqrt{-\eta}\cos\left[\frac{\varphi + 2\pi}{3}\right] - \frac{\lambda_1}{3}}; \\ &R_2 = \sqrt{2\sqrt{-\eta}\cos\left[\frac{\varphi + 4\pi}{3}\right] - \frac{\lambda_1}{3}}; \; \varphi = \cos^{-1}\left[-\varphi / \sqrt{-\eta^3}\right] \end{aligned} \tag{A.8}$$

ORCID iD

Suchart Limkatanyu https://orcid.org/0000-0002-4343-7654
Worathep Sae-Long https://orcid.org/0000-0001-8149-4409
Jaroon Rungamornrat https://orcid.org/0000-0002-2449-9067
Nattapong Damrongwiriyanupap https://orcid.org/0000-0001-7280-5957
Suraparb Keawsawasvong https://orcid.org/0000-0002-1760-9838
Piti Sukontasukkul https://orcid.org/0000-0002-9580-7063
Chayanon Hansapinyo https://orcid.org/0000-0002-6237-613X

How to cite this article: Limkatanyu S., et al. Static Bending Analysis of Nanobeam-Substrate Medium Systems Incorporating Mixture Stress-Driven Nonlocality, Surface Energy, and Substrate-Structure Interactions, *J. Appl. Comput. Mech.*, 11(2), 2025, 327-343. https://doi.org/10.22055/jacm.2024.47226.4679